修 士 論 文

Rapid Prototyping of a 12-Degree-of-Freedom
Underactuated Anthropomorphic Robot Hand

（ラピッドプロトタイピング用いた劣駆動
１２自由度ロボットハンドの開発）

平成 25年 8月 16日 提出

指導教員　　中村 仁彦 教授

116557　　トリーラッタナクンワオン　タナット
Treratanakulwong, Tanut

Master Thesis

Rapid Prototyping of a 12-Degree-of-Freedom Underactuated Anthropomorphic Robot Hand

The University of Tokyo

August 16, 2013

Advisor: Professor Yoshihiko Nakamura

116557 Treratanakulwong Tanut

Submitted to the Department of Mechano-Informatics of the Graduate School of Information Science and Technology in partial fulfillment of the requirements for the degree of

Master of Information Science and Technology

Contents

List of Figures

List of Tables

Chapter 1

Introduction

1.1 Background

The hand is one of the extremities that plays an important role in grasping and manipulating objects. In order to reproduce the human grasping functionality, the simple model of the hand consists of at least 20 degrees of freedom (DOF). [1]

To simplify large DOFs hands, some researchers study the coordination between finger joints in the human grasping motions, the so called "Synergies" [1, 2][3]. Furthermore the size of the robot hand has to be similar to the human hand to work in human environment. It means that all the actuators and transmission systems have to be carefully placed within very limited hand space.

Lots of interests are focused on the antropomorphic hand design. Gifu Hand [4] and HPR3 Hand [5] both are internal-actuation hand which joints are driven with small electric motors and high-reduction ratio gears which are located in the fingers. Later, DLR Hand [6] went one step beyond by adding torque sensor on every joints. Incorporating with control algorithms, DLR Hand can archive the soft grasping. To attain high grasping forces, the larger actuators and stronger reduction gears are required but consequently large motors do not fit into the hand.

An external-actuation hand is one possible solution where one can employ higher-power actuators outside the hand, e.g. forearm space. Utah/MIT

[1] Each finger has 3 DOFs for flexion-extension movement and 1 DOF for abduction-adduction movement. The thumb has more DOFs than the other fingers to achieve the complex movement. In total one hand consisted of at least 20 DOFs.

Hand [16, 7] has actuators outside the hand and transmit forces and motions through tendons. The main difficulty is how to deal with the routing of tendons. Recently, most of the hand designs are moving toward tendon-driven mechanisms [8][9].

Tendon-driven mechanisms can be classified into 3 categories depending on number of wires that connected with actuators. We denote N as the number of manipulator joints (DOFs). First, N-type has N actuators controlling N DOFs. The main issue is how to pretension the system to maintain positive tension force (pulling force) on the wires. $N+1$-type has $N+1$ tendons which are the smallest amount of tendons that is required to maintain positive tension and full controllability over N DOFs. Finally, $2N$-type has two antagonistic actuators controlling each joint. DLR Hand Arm System [8] uses $2N$-type tendon-driven mechanism with non-linear spring configurations on every joints to enable control over joint stiffness.

Underactuated hand is the design where controllable DOFs (number of actuators) are less than DOFs of the mechanism. Most underactuated hands have high adaptivity in power grasping where fingers can form the shape of objects. In the past, USC/Belgrade Hand [10] is one example where joint are coupled with rigid mechanical link. Lately, Catalano et al. [11] developed the synergy-driven robot hand with elastic elements. Using only few synergies, the hand can create most of the grasping patterns. Still, it is difficult for underactuated hands to exert pinching force for precision grasping.

1.2 Goals and Contributions of this Thesis

In this thesis, we are aiming at designing robot hand that has the similar functionality as the human hand but since the human hand is a very complicated system. We propose to reduce the system's complexity by considering the main functionality of human hand and design the mechanical system based on functions not the biological structure. Our design of the robot hand has 5 fingers with 19 joints driven by 12 active tendons. By introducing passive tendon coupling in underactuated design, we show that underactuated hand with our proposed coupling can preform better in fingertip pinching tasks. Rapid prototyping technology enables us to design a complex tendon-driven system that cannot be realized with conventional

material-removal machining process. The complex tendon-driven system, which actually has an inspiration from physiology, benefits in lowering the friction by avoiding sliding contacts. The prototype of our proposed robot hand has been made with rapid prototyping technology and test to prove our proposal on the design of robot hand based on human hand functionalities.

1.3 Rapid Prototyping Technology

Rapid prototyping is technologies that enable design to quickly fabricate the design from computer aided design (CAD) data. Instead of removing material by machining tools, called subtractive method, parts are fabricated with additive method where models are constructed by incrementally adding the material layer by layer. To do that, 3-dimensional (3D) CAD data are sliced into very thin layer represented by 2D drawing. Then, a special software generates the trajectory from 2D drawing and send them to the machine. This is when the fabrication is started.

Very well known and widely used rapid prototyping techniques are 3D printing, Selective Laser Sintering (SLS), and Stereolithography (SLA). Each technique has its own advantage and disadvantage as follows. 3D printing is based on extrusion of materials that can be melt. The material extruder move along X-Y plane to form a slice of the model and in addition after the completion of each layer the extruder (or building platform) moves along Z direction and the next layer is built. Thermoplastic materials ,e.g., Acrylonitrile butadiene styrene (ABS) or Polylactide (PLA), are often used which makes this process becomes very cheap and widely use. Next, Selective Laser Sintering (SLS) involves the use of a high power laser to fuse a small power of material (plastic, ceramic or metal) to form shapes. A roller delivers the next layer of powder on top of the previous one the laser beams are focused at the sintering area. The main advantage of this technique is very wide range of material can be used but still the resolution is less than that of Stereolithography (SLA) technology. In SLA, laser beams are used to cure the curable photopolymer. The product are strong enough to be machined later but the only difficulty is the choice of materials which have to be light curable. They often come with high cost.

1.4 Outline of Thesis

The outline of the thesis is organized as follows. First, we will look at robot hands that have been done so far in Chapter 2. We go into the detail of tendon-driven mechanism where the mathematical models, classifications, underactuated design, and coupling mechanism are discussed as well. Chapter 3 depicts our design principle which based on the physiology of human hand, low-friction pulley systems. The new coupling design for underactuated hand are proposed in this section. By the end, we consider types of tendon and the termination technique that will be used in our design. Later in Chapter 4, we review our design of anthropomorphic robot hand based on 3D-printing manufacturing process. An in detail mechanical design of each finger, palm and wrist are given. An implementation of joint encoders and how they are included inside the hand structure are explained. A prototype of the hand is built by 3D-printing process and experiment results are review in Chapter 5. Finally, conclusions are drawn in Chapter 6.

Chapter 2

Previous Researches on Tendon-Driven Robot Hands

2.1 Introduction

In this section, we will review the theory of tendon-driven mechanism started from building the mathematical model to describe tendon-driven mechanism and then the tendon-driven mechanisms are classified by using number of joints and number of actuators. More recent interests are moving towards underactuated design because underactuation reduces actuation complexity, resulting in a simpler system. For underactuated hand, it is important to review the concept of coupling. Coupling has an important role to relate the movement of one joint with the others.

2.2 Mathematical Model of Tendon-Driven Mechanism

To model the tendon-driven mechanism, let us denote n_{a} as the number of actuators, n_{j} as the number of joints, and n_{w} as the number of wires which constituted of n_{wa} active tendons and n_{wp} passive tendons. To distinguish the active tendons from the passive tendons, $\boldsymbol{x} \in \boldsymbol{R}^{n_{\mathrm{w}}}$ can be written as follows,

$$\boldsymbol{x} = (\boldsymbol{x}_{\mathrm{a}}^T, \boldsymbol{x}_{\mathrm{p}}^T)^T \tag{2.1}$$

where $\boldsymbol{x}_{\mathrm{a}} \in \boldsymbol{R}^{n_{\mathrm{wa}}}$ and $\boldsymbol{x}_{\mathrm{p}} \in \boldsymbol{R}^{n_{\mathrm{wp}}}$ are the displacements of active and passive tendons respectively. $\boldsymbol{q} = (q_1, \ldots, q_{n_{\mathrm{j}}})^T \in \boldsymbol{R}^{n_{\mathrm{j}}}$ is the joint space configurations of the manipulator. We can write the relation between $\dot{\boldsymbol{x}}$ and $\dot{\boldsymbol{q}}$ as follows,

$$\dot{\boldsymbol{x}} = J\dot{\boldsymbol{q}} = \begin{pmatrix} J_{\mathrm{a}} \\ J_{\mathrm{p}} \end{pmatrix} \dot{\boldsymbol{q}} \tag{2.2}$$

where $J \in \boldsymbol{R}^{n_{\mathrm{w}} \times n_{\mathrm{j}}}$ is the Jacobian matrix of joint velocities $\dot{\boldsymbol{q}}$ and velocity of tendons $\dot{\boldsymbol{x}}$. The Jacobian matrix composed of active-tendon Jacobian $J_{\mathrm{a}} \in \boldsymbol{R}^{n_{\mathrm{a}} \times n_{\mathrm{j}}}$ and passive-tendon Jacobian $J_{\mathrm{p}} \in \boldsymbol{R}^{(n_{\mathrm{w}} - n_{\mathrm{a}}) \times n_{\mathrm{j}}}$ which represent the Jacobian of elastic tendons.

The relationship between joint torques $\boldsymbol{\tau}$ and tension on the wires $\boldsymbol{f} = \begin{pmatrix} \boldsymbol{f}_{\mathrm{a}}^T & \boldsymbol{f}_{\mathrm{p}}^T \end{pmatrix}^T$ is below.

$$\boldsymbol{\tau} = J^T \boldsymbol{f} \tag{2.3}$$

$\boldsymbol{f}_{\mathrm{a}} \in \boldsymbol{R}^{n_{\mathrm{a}}}$ and $\boldsymbol{f}_{\mathrm{p}} \in \boldsymbol{R}^{n_{\mathrm{w}} - n_{\mathrm{a}}}$ are tension on actively-controlled tendon and tension on passive tendons respectively.

There exists a null space in J^T in the case of $n_{\mathrm{w}} > n_{\mathrm{j}}$. Then, the null space N is represented by arbitrary vector $\boldsymbol{\xi}$ in the following equation.

$$\boldsymbol{f} = (J^T)^{\#} \boldsymbol{\tau} + N\boldsymbol{\xi} \tag{2.4}$$

$(J^T)^{\#}$ represents the Moore-Penrose pseudoinverse of the Jacobian matrix J^T. In general, no compression force can be transmitted by tendons. To maintain positive tension forces on tendons $\boldsymbol{f} > \boldsymbol{0}$ in any joint torque configurations, it is necessary that there exists $\boldsymbol{\xi}$ such that $N\boldsymbol{\xi} > 0$. To satisfy previously mentioned condition, the least number of tendons required to control n_{j} DOFs manipulators is $n_{\mathrm{j}} + 1$ tendons or $n_{\mathrm{w}} \geq n_{\mathrm{j}} + 1$.

2.3 Classification of Tendon-Driven Mechanism

We classify tendon-driven mechanism by using the number of manipulator joints and the number of actuators. It is clear that if we wanted to control each joint independently the number of actuators (n_{a}) has to be at least the number of joints (n_{j}). For the following discussion, we consider the manipulators with N joints ($n_{\mathrm{j}} = N$). Tendon-driven mechanism can be classified into 3 types.

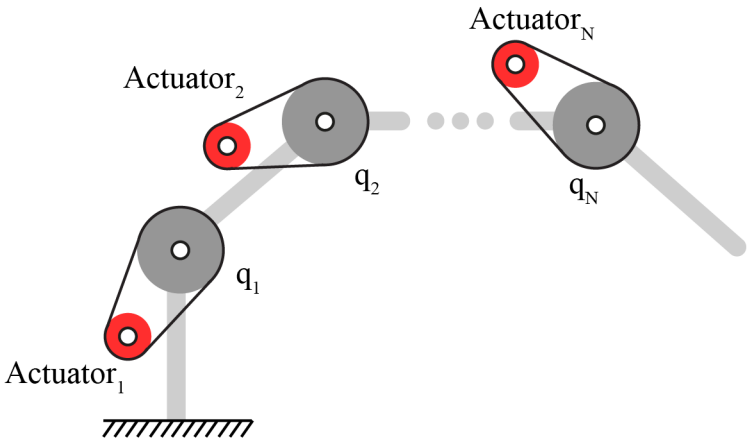

Figure 2.1: N-type tendon-driven mechanism on N joint manipulators with internal actuation.

2.3.1 N Type Tendon-Driven Mechanism

This type of manipulator has numbers of joints equal to number of actuators ($n_{\mathrm{j}} = n_{\mathrm{a}}$). This type of mechanism requires the least number of actuators $n_{\mathrm{a}} = N$. To actuate joints in both forward and reverse direction, it requires two tendons per each actuator to pull a joint in each direction. Consequently, the number of tendons are twice as much as the number of joints ($n_{\mathrm{w}} = 2N$). Pretension on tendons is necessary to prevent the tendons from being slack which would result in joints' backlash., Figure 2.1 shows N joints manipulator with this type of mechanism where red circles represent actuators and black lines are active tendons. More importantly, it is possible to put all actuators together in the root link of the manipulator. Figure 2.2 is an example of 3 joints manipulator which actuators are located at the base. This way, it is more practical in the design of robot hand because each link is too small to fit an actuator while we have enough space for actuators in forearm. Still, the main difficulty is how to manage $2N$ tendons through each joint without affected from joint movements.

2.3.2 N+1 Type Tendon-Driven Mechanism

According to Section 2.2, the least number of tendons for N joints manipulator is $n_{\mathrm{w}} = N+1$. To achieve full controllability over joint torques, at least $N+1$ actuators are required to drive all $N+1$ active tendons. The routing

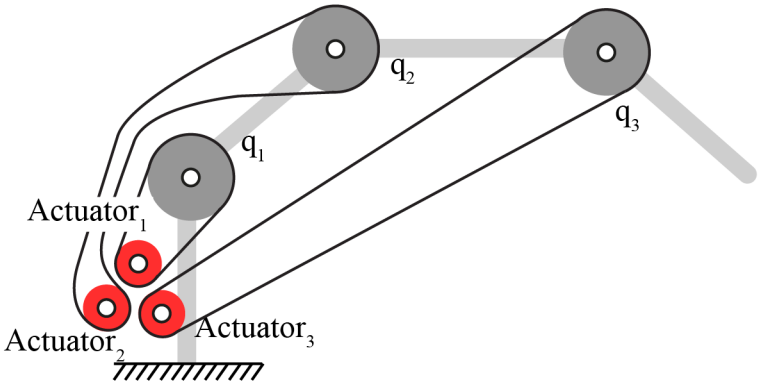

Figure 2.2: N-type tendon-driven mechanism on 3 joint manipulators with external actuation.

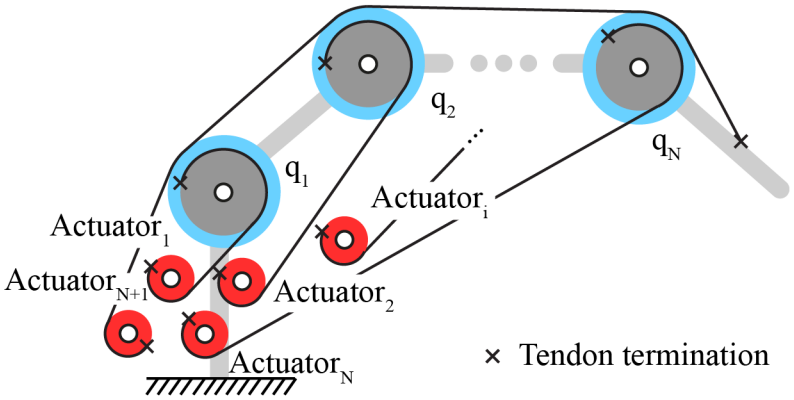

Figure 2.3: N+1 type tendon-driven mechanism on N joint manipulators.

of tendons has to be carefully chosen to be capable of maintaining positive tensions. Figure 2.3 shows one possible configuration of N+1 tendon-driven mechanism. Pulleys shown in blue are the idle pulleys while the gray pulleys are fixed to the next link of the manipulator. The termination of tendons can be any technique that fixes the end of tendon with the corresponding structure. This type of mechanism is famous of its reduction in number of transmission tendons which is the smallest number of tendons among all other types. However, it has main difficulty in control in which all the joint motions are coupled.

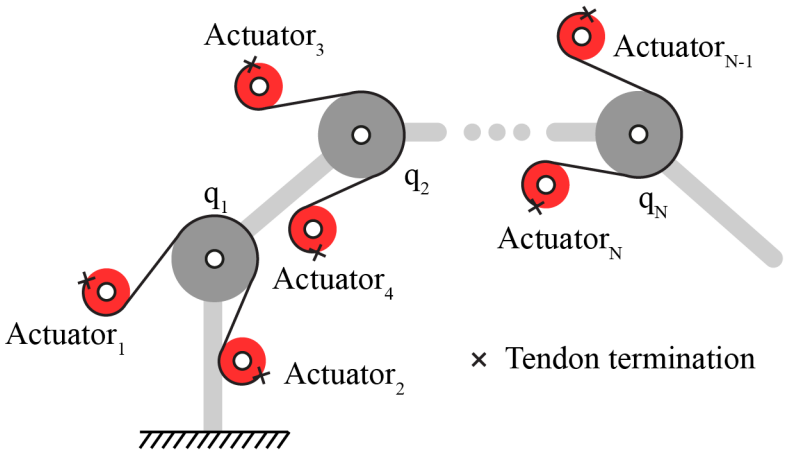

Figure 2.4: 2N-type tendon-driven mechanism on N joint manipulators.

2.3.3 2N Type Tendon-Driven Mechanism

Sometimes this type of mechanism is so called "Antagonistically tendon-driven mechanism". 2N-type uses the largest number of actuators which is two times the number of joints ($n_{\mathrm{a}} = 2n_{\mathrm{j}}$). Each joint is driven by 2 actuators. According to the fact that only positive tension can be transmitted on tendons, one actuator moves a joint in one direction and the other actuator moves the joint on the opposite. As a result, there are $2N$ tendons in total which is the same amount of tendons in N-type tendon-driven mechanism. This mechanism also requires no pretension system. Due to the redundancy of actuation of the system, some researchers also add non-linear spring configurations to enable control over joint stiffness. Figure 2.4 is one example of this type of mechanism. The drawbacks of this system are large number of transmission tendons and also huge number of actuators.

2.4 Underactuation for Robot Hands

Underactuation is a mechanism where Degree of Freedoms (DOFs) or number of joints (n_{j}) is larger than number of actuators (n_{a}) or in the other word $n_{\mathrm{j}} > n_{\mathrm{a}}$. This concept gains lots of interests recently because it reduces numbers of actuators which is costly in term of space in designing the robot hand and less actuators mean we can have the stronger ones that is demanded for the power grasping tasks.

There are more over 20 DOFs in human hand which means at least 20 actuators are required to independently control all DOFs in Fully-actuation case. Even though there are redundancy in the actuations of human hand, we cannot individually control some joints due to the tendon and muscle configurations but still human hand can form any object shapes after contact. With underactuation, we can build the robot hand with less DOFs to reduce complexity without reducing DOFs together with some mechanical constraints which determine underactuation behaviours.

The remaining questions for robot hand designers are at what level of human hand grasping and manipulation capability we wanted achieve with underactuated hand and if we wanted to reduce some actuators how the tendon transmission system should looks like.

2.5 Coupling Mechanism for Underactuated Hands

Most of the underactuated hand [9][11][12][13] have similar configurations of active tendons and passive tendons. In the case of 1-DOF finger with n joints, there is one active tendon ,going through all the joints and terminate at the fingertip, and n passive tendons connecting between any two neighbour links. There are $n+1$ tendons in total which is enough to maintain the positive tensions and uniquely determine the joint space configurations for any actuation. A coupling defines how the movement of each joint are related. In underactuated design with passive tendons, actuation forces are balanced with the force created by passive elements.

In order to do the analysis on the equilibrium configuration of underactuated hand when there is no external contact force, we reduce the model to underactuated finger with two joints, shown in Figure 2.5. There are three tendons composed of one active and two passive tendons. The active tendon is winded around the pulley to prevent it from losing the contact with pulley. The radius of pulleys of active tendon at joint q_1 and q_2 are $r_{\mathrm{a}1}$ and $r_{\mathrm{a}2}$. Two passive tendons have spring constants $k_{\mathrm{e}1}$ and $k_{\mathrm{e}2}$ with pretension x_1 and x_2. The passive tendons create moments around the joint by using idler pulleys with radius of $r_{\mathrm{e}1}$ and $r_{\mathrm{e}2}$.

After the finger is actuated with force F and displacement δl on an active tendon, the joint configuration of the system move to the new equilibrium at $\boldsymbol{q}' = (q_1 + \delta q_1, q_2 + \delta q_2)^T$. At the same time, the displacement of passive

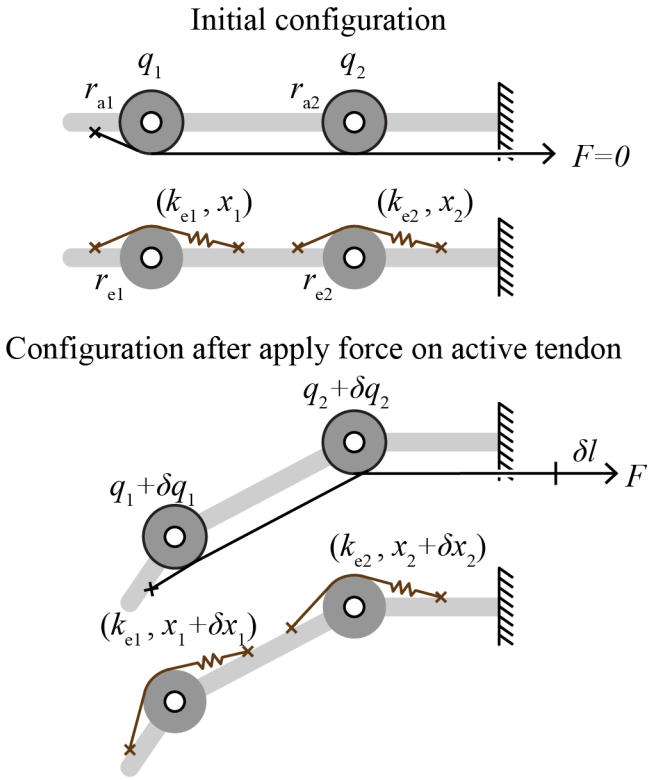

Figure 2.5: Configuration of active tendons and passive tendons for most of the underactuated hand design.

tendon also changed to $x_1 + \delta x_1$ and $x_2 + \delta x_2$ at the corresponding joint.

To identify the equilibrium joint position of the system, we do the analysis based on Virtual work method. At the equilibrium configuration, the total virtual work δU due to the external forces acting on the system is zero for any $\boldsymbol{\delta q} = (\delta q_1, \delta q_2)^T$.

$$\delta U = \frac{\partial V}{\partial \boldsymbol{\delta q}} = 0 \tag{2.5}$$

The potential function of the system after force F is applied to the active tendon can be written as follow,

$$\begin{aligned} \delta V &= \frac{1}{2}k_{e1}(x_1 + \delta x_1)^2 + \frac{1}{2}k_{e2}(x_2 + \delta x_2)^2 \\ &= \frac{1}{2}k_{e1}(x_1 + r_{e1}\delta q_1)^2 + \frac{1}{2}k_{e2}(x_2 + r_{e2}\delta q_2)^2 \end{aligned} \tag{2.6}$$

but actually the joint position δq_1 and δq_2 are not independent because the

routing of active tendon adds the following constrain to the system.

$$\delta l = r_{\mathrm{a}1}\delta q_1 + r_{\mathrm{a}2}\delta q_2 \tag{2.7}$$

Therefore, we can rewrite the equation 2.6 by substituting δq_2 from the above equation.

$$\delta V = \frac{1}{2}k_{\mathrm{e}1}(x_1 + r_{\mathrm{e}1}\delta q_1)^2 + \frac{1}{2}k_{\mathrm{e}2}(x_2 + r_{\mathrm{e}2}(\frac{\delta l - r_{\mathrm{a}1}\delta q_1}{r_{\mathrm{a}2}}))^2 \tag{2.8}$$

Virtual work method suggests the differentiation of equation 2.8 with respect to q_1 is equal to zero.

$$\frac{dV}{dq_1} = k_{\mathrm{e}1}r_{\mathrm{e}1}(x_1 + r_{\mathrm{e}1}\delta q_1) - k_{\mathrm{e}2}r_{\mathrm{e}2}\frac{r_{\mathrm{a}1}}{r_{\mathrm{a}2}}(x_2 + r_{\mathrm{e}2}(\frac{\delta l - r_{\mathrm{a}1}\delta q_1}{r_{\mathrm{a}2}})) = 0 \tag{2.9}$$

At the equilibrium we can show the relation between q_1 and δl as the following.

$$\delta q_1 = \frac{k_{\mathrm{e}2}r_{\mathrm{a}1}r_{\mathrm{e}2}x_2 - k_{\mathrm{e}1}r_{\mathrm{a}2}r_{\mathrm{e}1}x_1 + k_{\mathrm{e}2}r_{\mathrm{e}2}^2\frac{r_{\mathrm{a}1}}{r_{\mathrm{a}2}}\delta l}{k_{\mathrm{e}1}r_{\mathrm{a}2}r_{\mathrm{e}1}^2 + k_{\mathrm{e}2}r_{\mathrm{e}2}^2\frac{r_{\mathrm{a}1}^2}{r_{\mathrm{a}2}}} \tag{2.10}$$

We are interested in the configuration where all passive tendons have the same spring constant, same pretension levels and same moment arms. Therefore, we set $k_{\mathrm{e}1} = k_{\mathrm{e}2} = k_{\mathrm{e}}$, $r_{\mathrm{e}1} = r_{\mathrm{e}2} = r_{\mathrm{e}}$, and $x_1 = x_2 = x$. On the active tendon side, two pulleys have the same radius $r_{\mathrm{a}1} = r_{\mathrm{a}2} = r_{\mathrm{a}}$. The equation 2.10 results in simple form below.

$$\delta q_1 = \frac{\delta l}{2r_{\mathrm{a}}} \tag{2.11}$$

It is possible to calculate joint displacement q_2 as well by substituting q_1 from the above result on the equation 2.5.

$$\delta q_2 = \frac{\delta l}{2r_{\mathrm{a}}} \tag{2.12}$$

By doing analysis on the second derivative of potential function (d^2V/dq_1^2), it is possible to classify types of equilibrium. If d^2V/dq_1^2 is more than zero, the configuration where $dV/dq_1 = 0$ is minimum point resulting in stable equilibrium. On the other hand if d^2V/dq_1^2 is more than zero, the equilibrium condition is unstable. If all the higher order derivatives of potential function

is equal to zero, system is in the neutral equilibrium.

$$\frac{d^2V}{dq_1^2} = k_{\mathrm{e}1} r_{\mathrm{e}1}^2 + k_{\mathrm{e}2} r_{\mathrm{e}2}^2 \frac{r_{\mathrm{a}1}^2}{r_{\mathrm{a}2}^2} > 0 \tag{2.13}$$

Since the second order derivative of potential function is larger than zero, the resulting configuration $(\delta q_1, \delta q_2) = (\frac{\delta l}{2r_{\mathrm{a}}}, \frac{\delta l}{2r_{\mathrm{a}}})$ is the stable equilibrium configuration. For any actuation displacement δl, the equilibrium position always has $\delta q_1 = \delta q_2$ which we called them coupling effect.

For n-joint system with n passive tendons and one active tendon in the similar configuration to the one shown in Figure 2.5, it is possible to show the equilibrium configuration by using virtual work method as well. However, types of equilibrium can be computed by using the determinant value of $n \times n$ Hessian matrix.

Chapter 3

Design of Low-Friction Tendon-Driven Systems

3.1 Introduction

Friction is critical to the tendon-driven system because it changed the desired behaviour of the system, for example, it changes the equilibrium configurations, it degrades the force/torque controllability of the system. In this chapter, we look at the physiology of the human as an inspiration and more importantly, to review the functionalities of each component in the hand. Later, we discuss about how to achieve lower the friction in tendon-driven system by using pulleys instead of sliding contacts. We propose the new coupling design for underactuated hand that enhance fingertip pinching capability and we suggest the tendon-routing optimization for N+1 tendon-driven mechanism. Finally, choices of tendons and termination mechanism are given.

3.2 Physiology of Human Hand

3.2.1 Motion Notation of Human Hand

In physiology, there are words used to described the motion of the fingers. Figure 3.1 shows flexion and Extension movement of the fingers. Flexion movement is a movement where tips of the fingers are moving towards the palm while extension is moving in the opposite of flexion. The muscles that generate flexion movement of called flexor muscles and extensor muscles

in the other case. Adduction movement describe the movement of fingers towards the middle finger and abduction movement happens when fingers are spread around, shown in Figure 3.2.

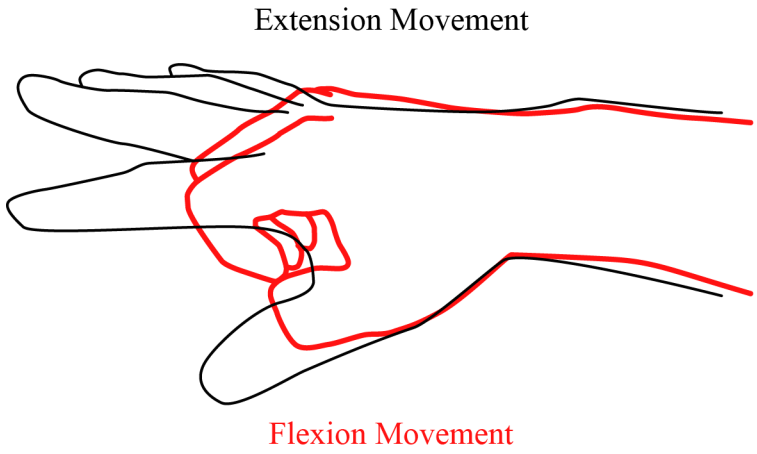

Figure 3.1: Flexion and extension movement of the fingers.

3.2.2 Fingers

Among all animals, hands attain perfection only in human due to its opposition movement [14]. Opposition is the movement which the pulp of the thumb is in contact with other fingers. The opposition movement can be seen even in great apes but the ranges are more limited compared to the human. Opposition of the thumb takes an important role in all grasping because the thumb is located almost opposite to the other four fingers so it enables force closure in any grasping.

Human hand consists of 27 bones and if we count both hands, the number of bones is over 20% of whole body bones. Figure 3.3 shows the configuration and naming of 27 bones of the right hand. Bones are classified in to 5 groups which are Distal Phalanges, Intermediate Phalanges, Proximal Phalanges, Metacarpals and Carpals. All four fingers, index/middle/ring/little, have almost the same structure which consists of 4 phalanges while thumb has only four phalanges. Lacking of Intermediate Phalanges in thumb resulting in a shorter thumb which benefits in opposition with all other fingers.

Joints are created with several shapes of bones and ligaments. Some researches in physiology have been done on the identification of joints [15]. Fig-

ure 3.4 is one way to simplify the joints in human hand. Trapezo-metacarpal joint (TM) is a 2-DOF joint that connect Metacarpal bone of the thumb with Trapezium bone on the wrist. 5 Metarpophalangeal joints (MCP) connect Metacarpal bones with the fist phalanges of the fingers. We simplify the MCP joints of index/middle/ring/little finger as 2-DOF joints because they are saddle joints with cylindrical surfaces [14] while MCP joint on the thumb has a very limited range of movement in one direction, therefore the MCP joint of the thumb is simplify with 1-DOF hinge joint. All Interphalangeal joint (IP), Proximal Interphalangeal joints (PIP) and Distal Interphalangeal Joints (DIP) are assumed to be 1-DOF hinge joint even though it can be observed in human that the rotation of these joint axis changes during the movement. It is important to remark here that our simplify model does not include DOFs for hollowing motion of the palm. Therefore, the hand consists of at least 20 DOFs.

Fibrous sheaths are the biologically designed pulleys that hold tendons in place and reduce the frictions that might generated from contact between tendon and bones. The existence of Fibrous sheaths can be seen on the palmar surface of Metacarpal bones, Proximal phalanges and Intermediate phalanges.

3.2.3 Palm

Palm of the human hand consists of several Metacarpal and Carpal bones. It is also an insertion place for some intrinsic muscles while at the same time it plays important role in routing all tendons of extrinsic muscles, muscles that are located outside the hand. From physiology, all extrinsic flexor muscles are guided through the concavities in side the palm which is made by arrangement of few Carpal bones [14]. The tunnel is called Carpal tunnel and on top of flexor tendons there is Flexor retinaculum that holds the tendon in place. Besides tendons, nerves are also guided along this tunnel. The illustration of Carpal tunnel and Flexor retinaculum is shown in Figure 3.5. Within the tunnel there is also Synovial sheaths that separate each tendon from surroundings which also prevent frictions that might occur in sliding contacts.

Some extensor muscles are also extrinsic muscles where tendons need to be routed through the wrist and palm. Figure 3.6 shows Extensor retinaculum that forms tunnels between itself and bones. Extensor tendons are also

routed within those tunnels. Again, the biologically design pulleys, Synovial sheaths, are also employed to reduce the frictions and control the tendons.

3.3 Low-Friction Pulley Systems

Human hands have lots of special structures such as, Fibrous sheaths and Synovial sheaths (previously mentioned in the Section 4.3.5), where the basic function is to change directions from one to the others. One similar structure that can be found in mechanical system is Bowden cable (the outer cable of the bicycle break line). By using Bowden cable, tendons (cables inside) can be guided anywhere that it is possible to bend the outer cable. Due to its simplicity in designing, Bowden cable is usually used in robot hands where many tendons from fingers are guided through palm and wrist [16, 17, 18, 19]. The main problem is occurrences of sliding contacts. When there are sliding contacts, the friction forces that is generated is proportional to the tensions on tendons and bending angles, resulting reduction of grasping force and controllability of tendon-driven systems.

One way to solve this problem is to use very low friction polymer materials, e.g, Polytetrafluoroethylene (PTFE) and Polyoxymethylene (POM) and reduce the sliding contact surface as much as possible. With a low friction plastic, the friction coefficient can go as low as 0.1. DLR Hand Arm System [20] is one example that the tendon routing parts are machined from low friction plastic. Still the estimation of tendon sliding friction is difficult and friction degrades both force sensitivity and backdrivability.

In the pulley based designs of tendon-driven mechanism, there is no sliding contact between tendons and pulleys. With the use of bearings, pulleys are supported with ball bearings where the inner diameter of bearings is fixed to shafts. Inside bearings, there are many balls rolling along the groove between inner diameter and outer diameter. It can be seen that there exists no sliding contact in pulley systems which resulting in much less friction compared to the systems with sliding contacts. Utah/MIT hand [7] is an attempt in the past to overcome sliding contacts by twist and bend tendons trough the pulley. Still the level of complexity of pulley system is limited by the machining techniques at this time. The recent design of highly underactuated 20 DOF robot hand, that is driven by only one actuator, is also based on the pulley systems but still pulleys are oriented on orthogonal

planes.

We proposed to reduce the use of sliding contacts by replacing them with pulleys. For any arbitrary directions and location of lines, it is possible to construct one line that connects two previous lines. Using all 3 lines, 2 planes made by lines next to each other can be formed. Here, those 2 planes represent the plan of pulleys. As a result, we can use 2 pulleys in 3-dimensional arbitrary planes to route tendon from and to any directions and locations in 3D space.

Figure 3.7 show the comparison between tendon routing with sliding contacts and our proposed pulley systems. Two low friction plastic bushings on the left is replaced with pulley system on the right. Both two configuration has the same entrance and exit location-orientation of the tendon.

3.4 Proposed Design of Coupling

Most of the underactuated hand [9][11][12][13] have similar configurations of the passive elements (elastic bands), shown in 3.8(a). The implementation of this method is simple. When the active wire is being pulled, the equilibrium joint configurations can be interpret as the configuration that has minimum potential energy which is previously discussed in Section 2.5. However, in the pinch grasping situation, where contact forces happen at the finger tip, the amount of deformation depends on the spring constant. When we want to exert larger finger tip forces, the higher-stiffness springs are required. Therefore, actuators need to generate larger forces to overcome spring forces and as a result maximum grasping force is lower unavoidably.

The new coupling mechanisms that we proposed are based on the following ideas.

1. The extension springs have the lowest possible stiffness which is enough just to prevent the finger from moving due to the gravity.

2. Increase the fingertip forces.

3. The finger does not lose any capability in adapting to the object shape.

Our proposed mechanism is shown in 3.8(b). The blue lines represent extension springs, the red lines are joint-coupling spring. If the red spring has an infinite stiffness, two joints will become 1 DOF, for example, $q_1 = q_2$ is always hold. In the proposed mechanism, the blue springs are those with high

stiffness for joint coupling while the red ones have as low stiffness as possible for extension of the finger. The joint configuration is uniquely determined. The underactuation is shown when large contact forces are exerted on to the finger. With our proposed design, it is possible to selectively choose the spring constants of extension springs and coupling springs.

For the following discussions, R_i is the radius of pulley where i is e for extension pulley, c for coupling pulley and a for actuator pulley. Using the same definition, we can write k_{e} as the extension-spring constant and k_{c} as a coupling-spring constant.

Given the coupling mechanism in 3.8(b), the relation between tendon lengths $\boldsymbol{x} = \begin{pmatrix} l_{\mathrm{a}} & l_{c1} & l_{c2} & l_{e1} & l_{e2} \end{pmatrix}^T$ and joint angles $\boldsymbol{q} = \begin{pmatrix} q_1 & q_2 \end{pmatrix}^T$ is the following.

$$\dot{\boldsymbol{x}} = J\dot{\boldsymbol{q}} = \begin{pmatrix} R_{\mathrm{a}} & R_{\mathrm{a}} \\ R_{\mathrm{c}} & -R_{\mathrm{c}} \\ -R_{\mathrm{c}} & R_{\mathrm{c}} \\ -R_{\mathrm{e}} & 0 \\ 0 & -R_{\mathrm{e}} \end{pmatrix} \dot{\boldsymbol{q}} \tag{3.1}$$

When the position of actuator is fixed, $\dot{l_{\mathrm{a}}} = 0$. the external force $\boldsymbol{P}$ exerts on the finger and moves the finger to the new configuration $\boldsymbol{q} + \boldsymbol{\delta q}$. The work done by external force W_{ext} transforms into an energy stored in the system as follows:

$$W_{\mathrm{ext}} = \frac{1}{2}\boldsymbol{\delta q}^T (J^T K J)\boldsymbol{\delta q} \tag{3.2}$$

where $K_{\mathrm{qb}} = J^T K J$ is the joint stiffness of all passive tendons which equals to,

$$K_{\mathrm{qb}} = \begin{pmatrix} 2R_{\mathrm{c}}^2 k_{\mathrm{c}} + R_{\mathrm{e}}^2 k_{\mathrm{e}} & -2R_{\mathrm{c}}^2 k_{\mathrm{c}} \\ -2R_{\mathrm{c}}^2 k_{\mathrm{c}} & 2R_{\mathrm{c}}^2 k_{\mathrm{c}} + R_{\mathrm{e}}^2 k_{\mathrm{e}} \end{pmatrix} \tag{3.3}$$

We can simply derive the joint stiffness matrix of the mechanism in Figure 3.8a as K_{qa} by setting the stiffness for coupling tendon zero $k_{\mathrm{c}} = 0$

$$K_{\mathrm{qa}} = \begin{pmatrix} R_{\mathrm{e}}^2 k_{\mathrm{e}} & 0 \\ 0 & R_{\mathrm{e}}^2 k_{\mathrm{e}} \end{pmatrix} \tag{3.4}$$

Considering the equation (3.3), when $q_1 = q_2$, (desired coupling trajectory) the work done by external force transformed into the energy stored by

only spring k_{e} while on the other hand when $q_1 \neq q_2$ energies are stored in both extension spring and coupling spring. The elastic energy are restored when the external forces is removed and the finger moves back to the original configuration $q_1 = q_2$

As an illustrating example for 2-joints coupling, we can extend the same idea to 3-joints coupling as shown in the Figure 3.9. All the constrains tendon in orange are three independent linear constrains which do not require any work done to move along coupling trajectory. As a result the trajectory $q_1 = q_2 = q_3$ is desired when there is no external force acting on the system.

A similar coupling mechanism for 2 joints with 1 DOF was proposed by Ozawa et al. [21] but the main difference is they model the extension tendon as an active tendons while passive tendons in our case. To summarise, our proposed design enables both precision and power grasping. We proposed to reduce the active DOFs by using extension spring and finally we introduces the coupling for 3 joints 1 DOF.

3.5 Tendon-Routing Optimization for N+1 Tendon-Driven Mechanism

For N+1 type tendon-driven mechanism, there are many tendon routings that satisfy the necessary condition of tendon-driven system where all tendons has positive tensions in any joint torque configurations. In order to choose one of the tendon routings, we specify a criteria for good tendon routing and perform the optimization.

Assuming a manipulator with n_{w} wires and n_{j} joints, we can write $n_{\mathrm{w}} = n_{\mathrm{j}} + 1$ by the definition of N+1 tendon-driven mechanism. To perform n_{j} - DOF of torque controllability all n_{w} have to be active tendons. We can write the relation between tension forces ($\boldsymbol{f}$) and joint torques ($\boldsymbol{\tau}$) as follows,

$$\boldsymbol{\tau} = J(\mathrm{x})^T(\boldsymbol{f} + \boldsymbol{f}_{\mathrm{b}}(\mathrm{x})) \tag{3.5}$$

where $J(\mathrm{x})$ is the Jacobian matrix of distinct tendon configuration x and $\boldsymbol{f}_{\mathrm{b}}(\mathrm{x})$ is the force bias that lies in the null space of $J(\mathrm{x})^T$, denoted by $Null(J(\mathrm{x})^T)$. It has been shown in Section 2.2 that $\boldsymbol{f}_{\mathrm{b}}(\mathrm{x}) > \mathbf{0}$ is a necessary condition to maintain positive tension forces on any joint torque configurations. We define a criteria for good tendon routing as tendon routing that has

the most uniform force bias. Therefore, we denoted $\boldsymbol{e} = 1/\sqrt{n_{\mathrm{w}}}(1, 1, \ldots, 1)^T$ as a n_{w}-dimensional uniform bias vector. The following objective function is used in the optimization routine to find good candidates of tendon routing.

$$\begin{aligned} \underset{x}{\text{maximize}} \quad & \boldsymbol{e}^T \frac{\boldsymbol{f}_{\mathrm{b}}(\mathrm{x})}{|\boldsymbol{f}_{\mathrm{b}}(\mathrm{x})|} \\ \text{subject to} \quad & \boldsymbol{f}_{\mathrm{b}}(\mathrm{x}) > \mathbf{0} \text{ and } \boldsymbol{f}_{\mathrm{b}}(\mathrm{x}) \in Null(J(\mathrm{x})^T) \end{aligned} \tag{3.6}$$

The main reason why uniform bias force is demanding because we assumed that all actuators have the same power capability. Therefore, to balance the loads among actuators the bias forces have to be uniform as well. In the case of non-identical actuators, we can still perform the same optimization routine by adding the weighed bias force on $\boldsymbol{e}$ to weighted the powerful actuators with the others.

3.6 Tendon

3.6.1 Tendon Material

In tendon-driven mechanism, tendons have a main role in transmitting movements from actuators to joints. The ideal properties of the tendons are able to withstand large force while having very small elongations. Stainless steel wires are usually very strong but heavy while tendons made from polymer are much lighter but most of them are not as strong as the steel wires. Ultra High Molecular Weight Polyethylene (UHMWPE) is a thermoplastic polyethylene which can goes over 15 times stronger compared to steel at the same weight [22]. Among these high performance tendons, there are several trademarks, such as Dyneema™, Zylon™, and Vectran™[23]. Zylon™is the strongest one but its strength decreases after few weeks of using due to hydrolysis, a chemical reaction with vapour in the air resulting in degrading the polymer. The second strongest among the class is Dyneema™which is widely use in tendon-driven robot hand [18][8]. It has no hydrolysis reaction, good UV resistance, low friction and good abrasion resistance.

Dyneema™DB-56HSL from Hamilon Company [23] is made of 8 strands Dyneema™fibers. At the 1.5 mm diameter, it can withstand around 2865 N, shown in Figure 3.10. The right figure illustrates 8 stands braiding of 1.5 mm tendon.

3.6.2 Tendon Termination

One way to fix the tendons with the finger structures is by making a knot. Here, we are considering only at knots that form loops at the end of tendons. Later, we will design the part to fix the loop with the structure. There are lots of available techniques to make the loop. Uniknot, Surgeon's loop and Butline hitch are examples of the knot that prevent themselves from loosing with the frictions on tendon surfaces. However, those knots tend to slips due to the low friction characteristic of Dyneema™. Long bury splice and Brummel splice are alternatives where loops are locked by tendon braiding. Long bury splice is made by separating the strands and braid each single strand into the tendon itself which is actually vary strong but not rarely works with very thin fibre tendons because of the difficulty in knitting.

Brummel splice is a knotting technique which works by making loop with strand-locking technique . The procedure to make Brummel splice is illustrated in Figure 3.11. First, make the blue mark on short end of tendon and red mark on long end of tendon. A distance between two marks represent the circumference of the resulting loop, shown in yellow part of the tendon. Secondly, separate the stands at the read mark into two groups equally and insert the short end of the tendon into the hole. Then, separate the stands again at the blue mark and put the long end into the hole. Finally, apply the stress on to the long end and the loop to make the knot tight. Later in the next chapter, we will show the strength test result of Brummel splice in comparison with others conventional knotting technique.

In the real utilization of the knot, not always that we can have both free ends, for example, when we made Brummel splice on one end of a tendon and fix it to the finger structure. Still, we need to make a loop at the other end of the tendon to hook it with actuators which means a knotting technique that requires only single free end of the tendon is necessary. We develop a knotting technique to make the same Brummel splice knot with only one free-end tendon. The process is shown in Figure 3.12. This process is indeed the reverse process of building Brummel splice with two free end. This time we start separating the strands from the short end (blue one). Then, at the III step, a section of the tendon is pushed through the open hole and repeating the same step on the red mark. Finally at the VII step, it ends up at the same result apart from the III and VI steps where separated strands are twisted which is negligible because twisting can be prevented by

pre-twisting the tendon in the opposite direction.

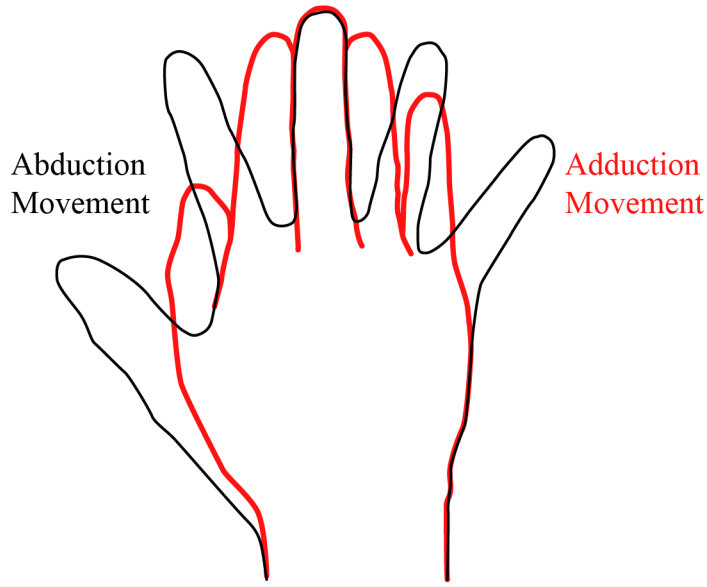

Figure 3.2: Adduction and abduction movement of the fingers.

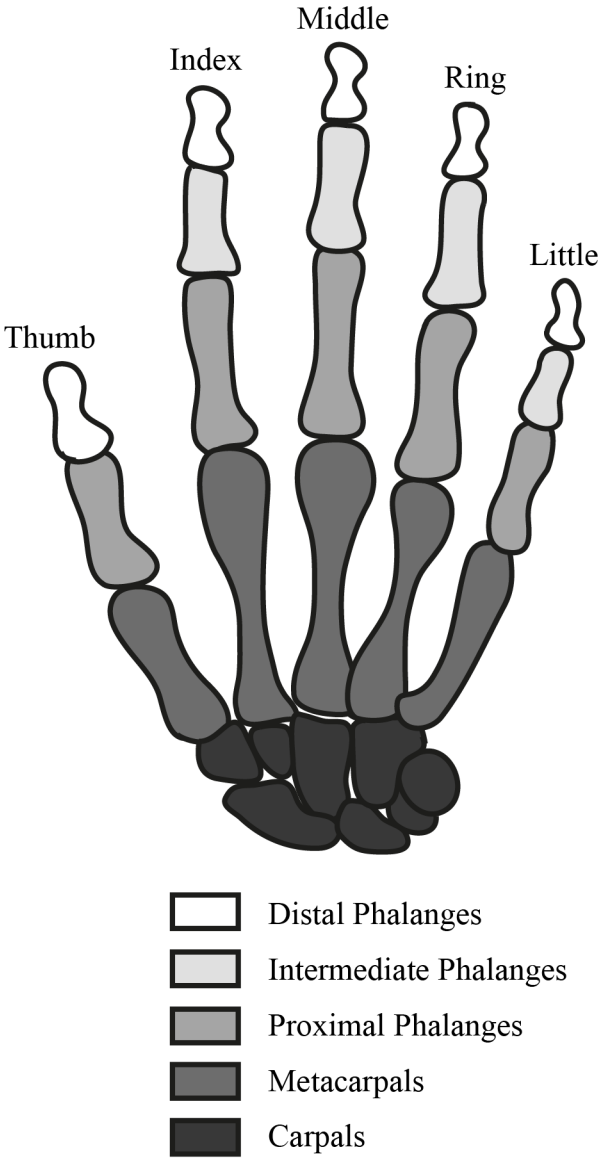

Figure 3.3: Bones of the right hand.

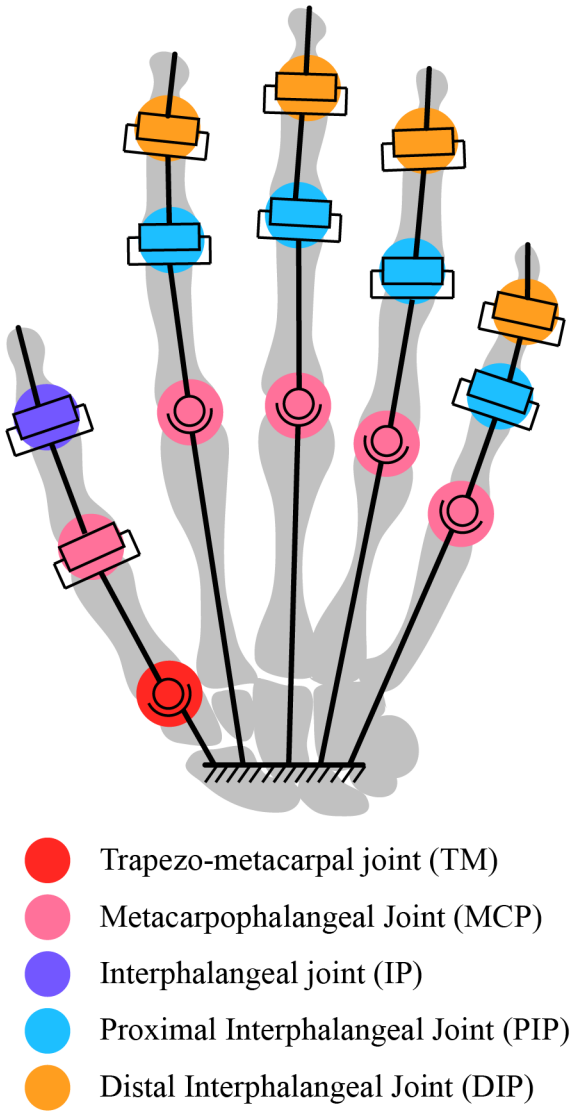

Figure 3.4: The simplify joint configuration for human hand.

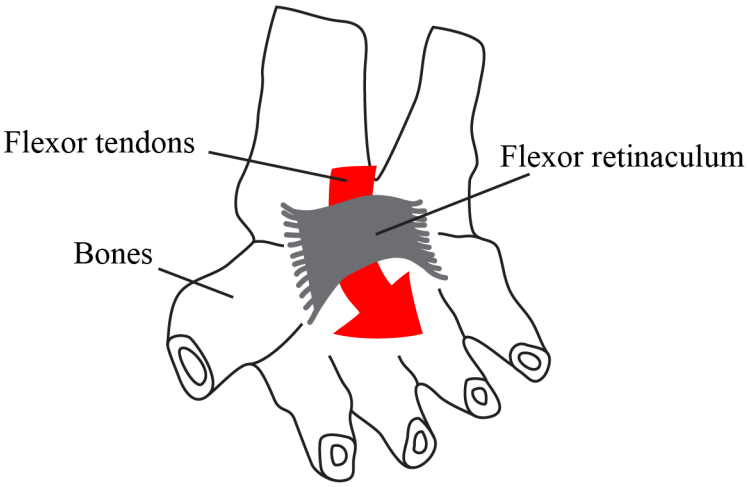

Figure 3.5: Carpal tunnel of a right hand where flexor tendons are routed inside.

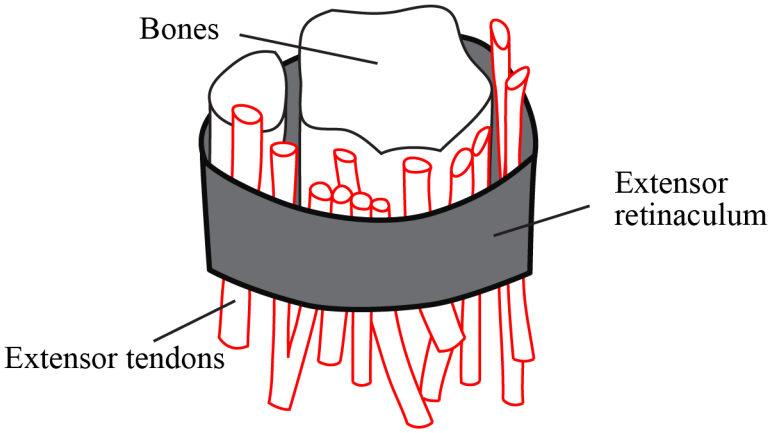

Figure 3.6: Extensor retinaculum of a right hand routing extensor tendons.

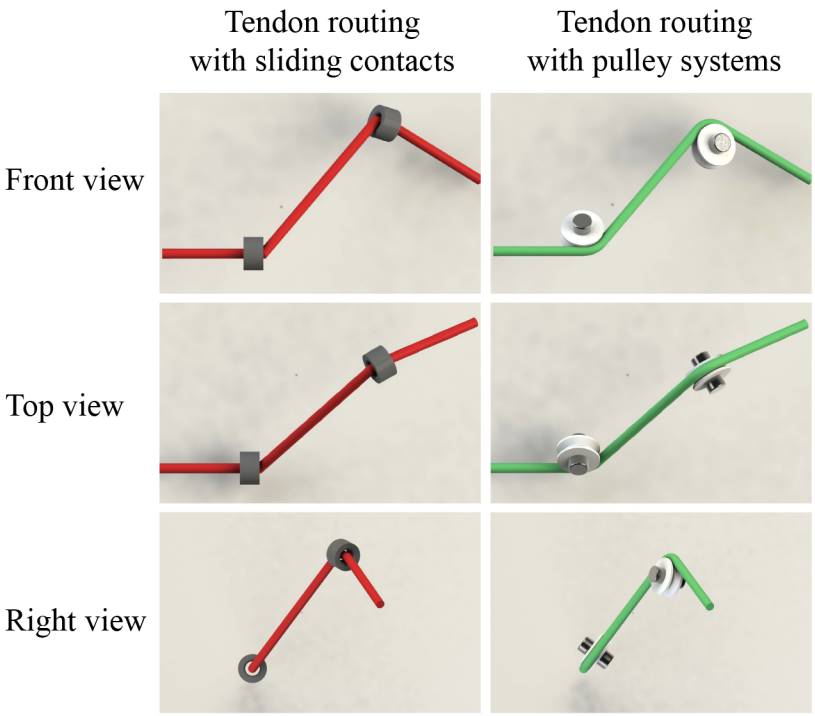

Figure 3.7: Comparison between tendon routing with sliding contact and pulley system.

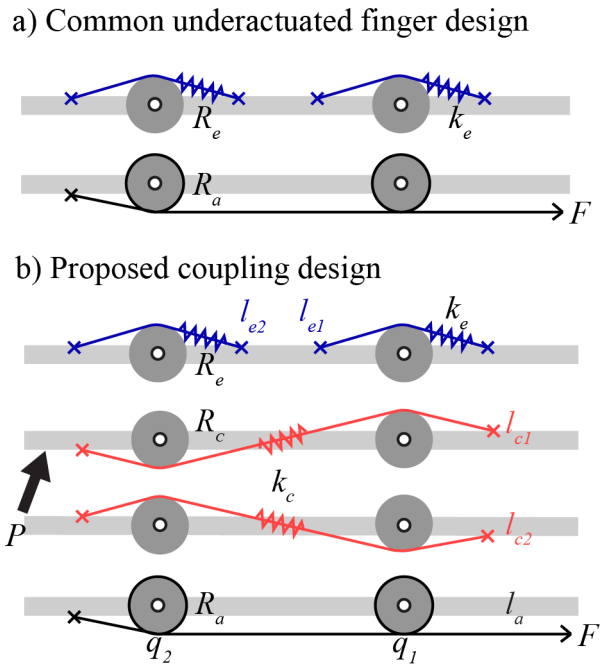

Figure 3.8: The configuration of active and passive tendons (a) The popular design of underactuated hand.(b) The proposed design of coupling mechanism for 2 joints with 1 DOF. Blue lines are passive extension tendon, red lines are passive coupling tendons and back lines are active tendons.

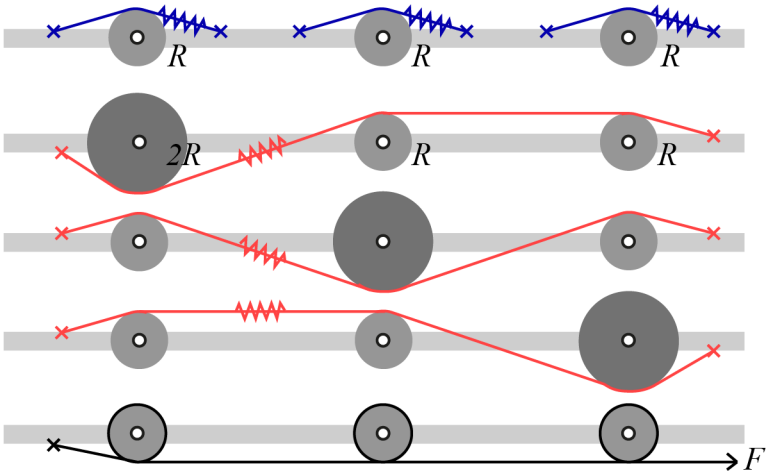

Figure 3.9: The proposed design for 3 joints coupling with 1 DOF.

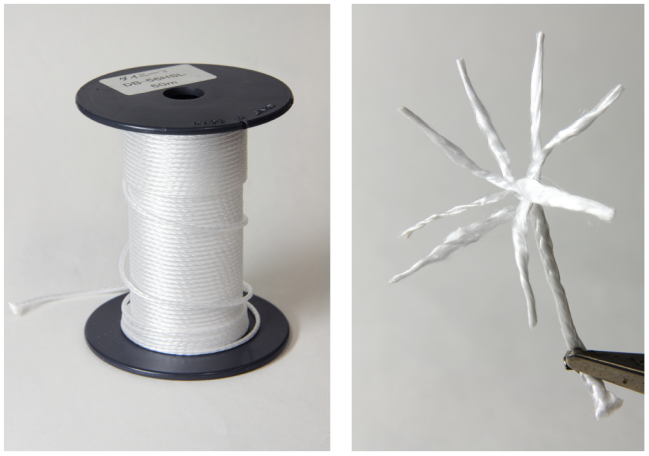

Figure 3.10: DB-56HSL 1.5 mm Dyneema™tendon from Humilon Company.

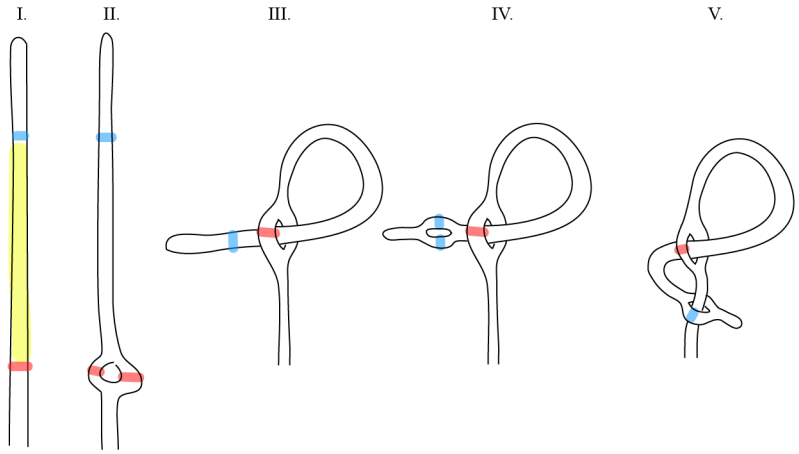

Figure 3.11: The process to make Brummel Splice with two free-end tendon.

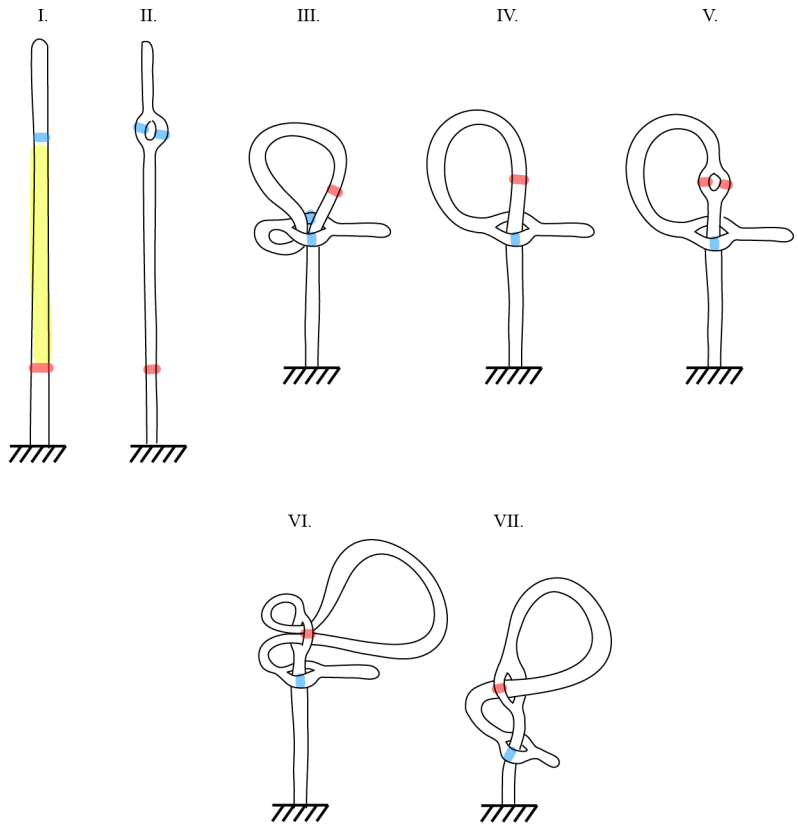

Figure 3.12: The process to make Brummel Splice with one free-end tendon.

Chapter 4

Design of Anthropomorphic Robot Hand

4.1 Introduction

By using human physiology as an inspiration, we proposed the design of robot hand that has similar functionality as the human hand. The design is based on one of a rapid prototyping technology, called 3-dimensional printing. With this manufacturing process, it enables the free-form design of pulley systems that cannot be fabricated with any conventional process. We discuss into detail about mechanical design of each fingers, palm, and wrist. From the beginning we included the design of joint angle sensors in the finger structures.

4.2 3D-Printing Based Design

Anthropomorphic robot hand design does not mean only building a robot hand that resembles the functionalities of human hands but also a robot hand that has similar structure and size when comparing with the human one. Material-removal machining process starts with a solid material and then the milling head remove the material from out side little by little which makes it impossible to design the product with under-cut. On the contrary, 3D-printing process enables building any shapes even the design is not accessible from outside.

To explore the new design space which is mechanically meaningful and

the shapes that cannot by any conventional process, it is true that parts which are intended to build with machining process can be build with 3D-printing process while the contrary is not true. 3D-printing process enables us to design parts not only from outside but the detail inside the parts can be manufactured. One direct benefit is that we reducing number of parts by combining many neighbour parts. As a result, the products have more reliability and assembly counts become less.

Though 3D-printing process facilitates designers in building fast prototype, it has a very strict limitation in resolution and accuracy while in the conventional process tolerances can be specify to make the products very precise. We developed a common design procedure to attain the good fitting of final products manufactured with 3D-printer. We specify the part clearances based on the shapes and printing machine. For some holes that require all precision required detail are machined afterwards. Finally, we adopted some special treatments on 3D-printed parts to increase the strength.

4.3 Mechanical Design

The main structure of our robot hand design is divided into five main components, see Figure 4.1. All five fingers are categorized into 3 groups, which are index / middle finger, little / ring finger and thumb, that results into 3 type of components. Every fingers has origins on the palm which also has role in preparing the direction before enter the wrist. Finally, the wrist has no DOF but again converting the direction and position before tendons connect to 12 linear actuators.

In this section, we first introduce the design of pulley systems without tendon winding which usually results in generating friction. Then, we will go into the design concept of each main components starting from index and middle finger, little and ring ringer, thumb, palm, and wrist.

4.3.1 Pulley Systems

Most of the times conceptual drawing of the pulley systems can be drawn in the similar manner of the one shown in Figure 4.2. Consider rotational joint j of the finger, the tendon i is winded around the pulley with r_{ij} radius. Linear displacement δx_i due to changes in joint angle δq_j is explained by the

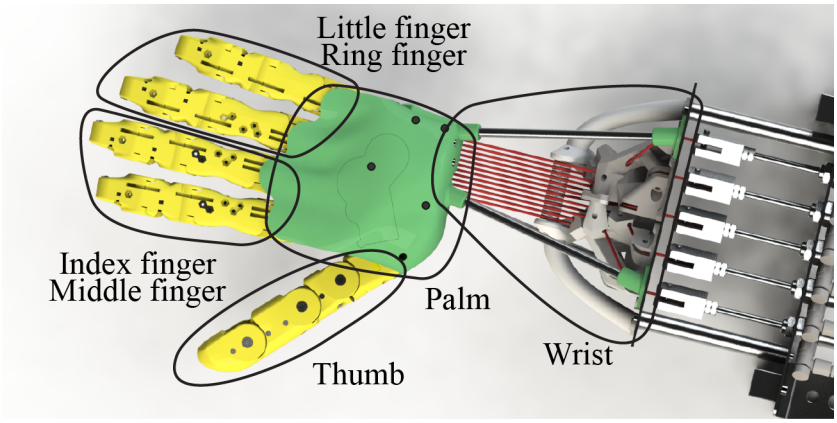

Figure 4.1: Five main components of the hand.

following relation.

$$\delta x_{\mathrm{i}} = r_{\mathrm{ij}} \delta q_{\mathrm{j}} \tag{4.1}$$

It is necessary to keep contacts between any tendons and the corresponding pulleys to create a constant moment arm. To prevent tendons from running out of the grooves of pulleys, tendons must be winded one time around the pulley. The grooves on pulleys have to be at least two times the diameter of tendons which increase the pulley thickness. Similar implementations on the tendon-driven robot hand can be found in [11]. The main problem of this approach is the collisions between winded tendons which results in friction.

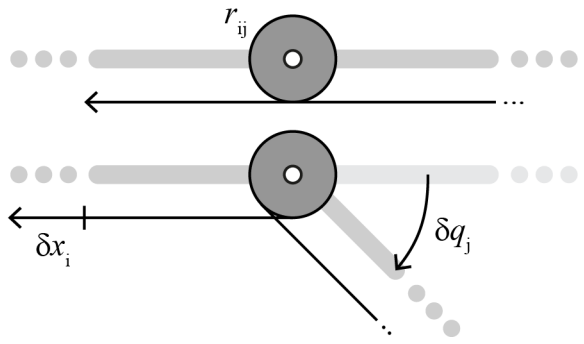

Figure 4.2: Pulley system with tendon winding.

The other way to route the tendon without winding [7, 9] is presented in Figure 4.3. In order to maintain contact between tendon and pulley, two idler pulleys, drawn in red, are fixed to adjacent links. Since there is no

winding, no friction is generated from collision of tendons. With proper sizes and position of those idler pulleys, the pulley systems behave the same as with winding. The possible configurations of idler pulleys that can maintain contact during the whole range of movement have to satisfy the following in equality,

$$\alpha_1 + \alpha_2 \geq \theta_{\max} \tag{4.2}$$

where $\theta_{\max}$ is the maximum angle of joint rotation relative to the joint's zero position and α_1,α_2 are the angles of tendon, as shown in Figure 4.4. In the following tendon-driven hand, we employ the pulley system without winding to reduce frictions and idler pulleys help prevent tendons from derailing.

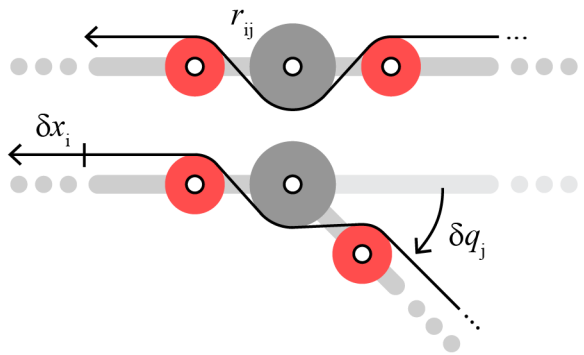

Figure 4.3: Pulley system without tendon winding.

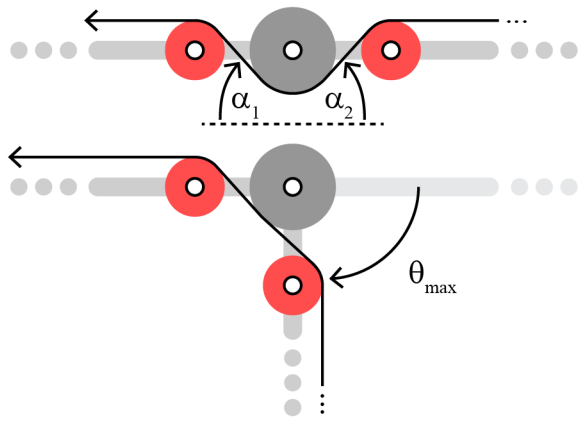

Figure 4.4: The proper location of idler pulleys that can maintain contact between tendon and joint's pulley without winding.

4.3.2 Index Finger and Middle Finger

According to the simplified model of human hand in Section 3.2.2, we design index and middle finger with the same mechanism. They both are important in finger tip pinching tasks which require an independent control over flexion of MCP joint and PIP joint while it is possible to observe that DIP and PIP joint are coupled in human. Here, we implement our proposed coupling mechanism for underactuated hand from Section 3.4. To design two-DOF joint of MCP, we split it into MCP1 and MCP2 where MCP2 creates flexion and extension movement while MCP1 creates abduction and adduction movement. We take the range of movement as a design specification for those two fingers, described in Table 4.1. We decided to fix MCP1 joint of the middle finger to the palm to be the center of adduction. We will go into the design of MCP1 joint later in Section 4.3.5.

Table 4.1: Movement ranges of index and middle finger.

Fingers	DIP	PIP	MCP2	MCP1
Index	0° to 90°	0° to 90°	0° to 90°	0° to 20°
Middle	0° to 90°	0° to 90°	0° to 90°	0°

A tendon routing of index finger is shown in Figure 4.5. Three joints in flexion plane are denoted by DIP, PIP, and MCP2. Index finger is controlled by two active tendons called Index DIP which ends at the distal phalanx while Index MCP2 which ends at the proximal phalanx. There are 5 passive tendons which can be categorized as 2 passive tendons for coupling (x_{c1} and x_{c2}) and the other three for extension movement (x_{e1}, x_{e2}, and x_{e3}). All three passive tendons for extension have the same spring constant k_e and k_c for coupling tendons. We can express $\dot{\boldsymbol{x}}$ and $\dot{\boldsymbol{q}}$ as follows,

$$\dot{\boldsymbol{x}} = (\dot{x}_{\text{Index DIP}},\ \dot{x}_{\text{Index;MCP2}},\ \dot{x}_{c1},\ \dot{x}_{c2},\ \dot{x}_{e1},\ \dot{x}_{e2},\ \dot{x}_{e3})^T \tag{4.3}$$

$$\dot{\boldsymbol{q}} = (q_{\text{DIP}},\ q_{\text{PIP}},\ q_{\text{MCP2}})^T \tag{4.4}$$

where we can derive the relation between those two variable with regards to tendon routings in Figure 4.5.

$$
\begin{aligned}
\dot{\boldsymbol{x}} &= J\dot{\boldsymbol{q}} \\
&= \begin{pmatrix}
r_{\mathrm{a1}} & r_{\mathrm{a1}} & r_{\mathrm{a1}} \\
0 & 0 & r_{\mathrm{a2}} \\
-r_{\mathrm{p1}} & r_{\mathrm{p1}} & 0 \\
r_{\mathrm{p1}} & -r_{\mathrm{p1}} & 0 \\
-r_{\mathrm{p2}} & 0 & 0 \\
0 & -r_{\mathrm{p2}} & 0 \\
0 & 0 & -r_{\mathrm{p2}}
\end{pmatrix} \dot{\boldsymbol{q}}
\end{aligned}
\tag{4.5}
$$

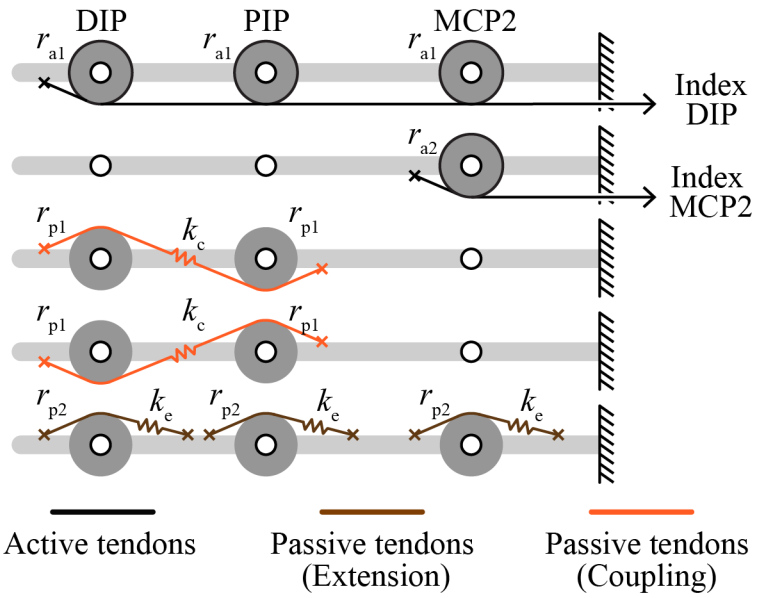

Figure 4.5: Tendon routing of index and middle finger.

To prevent the collision of tendons due to tendon winding in Figure 4.5, we add idler pulleys using the concept described in Section 4.3.1, shown in Figure 4.6. The pulleys shown in red are idler ones.

The section view of index finger is illustrated in Figure 4.7. Extension passive tendons is shown in brown. Even though one one brown tendon is drawn, the design allows separations of the brown tendon into 3 independent tendons (x_{e1}, x_{e2}, and x_{e3}) by using the tight fitting groove on intermediate phalanx and proximal phalanx. The extension passive tendons and two active tendons are stacked on the same section layer in the design to save a space while two other passive tendons for coupling are located on two

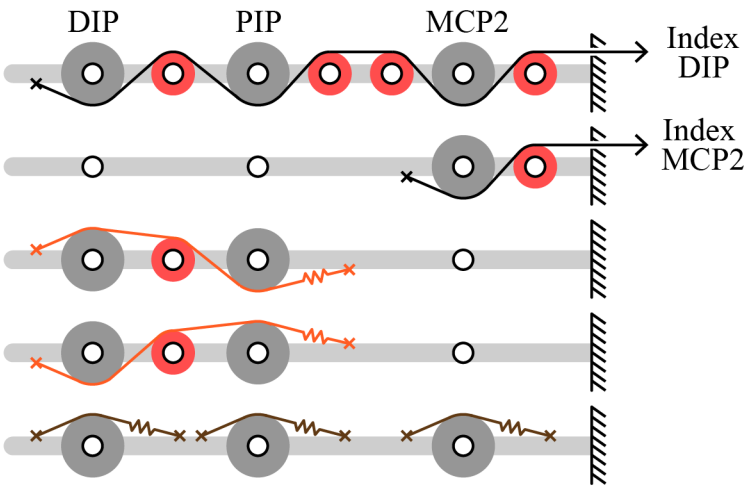

Figure 4.6: Tendon routing of index and middle finger without winding.

separate layers. All pulleys are ball-bearing supported to reduce the friction.

4.3.3 Little Finger and Ring Finger

Little and ring finger have the same design but different proximal phalanx length to replicate the length of human fingers. Ranges of movement in flexion plane are similar to that on the design of index and middle finger but the range of MCP1 joints are differ between little and ring finger. Table 4.2 depicted the movement ranges of little and ring finger.

Table 4.2: Movement ranges of little and ring finger.

Fingers	DIP	PIP	MCP2	MCP1
Ring	0° to 90°	0° to 90°	0° to 90°	0° to 10°
Little	0° to 90°	0° to 90°	0° to 90°	0° to 20°

They are underactuated design with 3 flexion joints (DIP, PIP, and MCP2) driven by only one active tendon. Three joint coupling mechanism, as described in Section 3.4, provides constraints on movement over underactuated fingers. The routing of tendons is shown in Figure 4.8. Three orange lines are passive tendon for coupling, denoted by x_{c1}, x_{c2}, and x_{c3}. The other three passive tendons for extension of the fingers are drawn in brown, namely x_{e1}, x_{e2}, and x_{e1}. By using a similar approach as we did in the

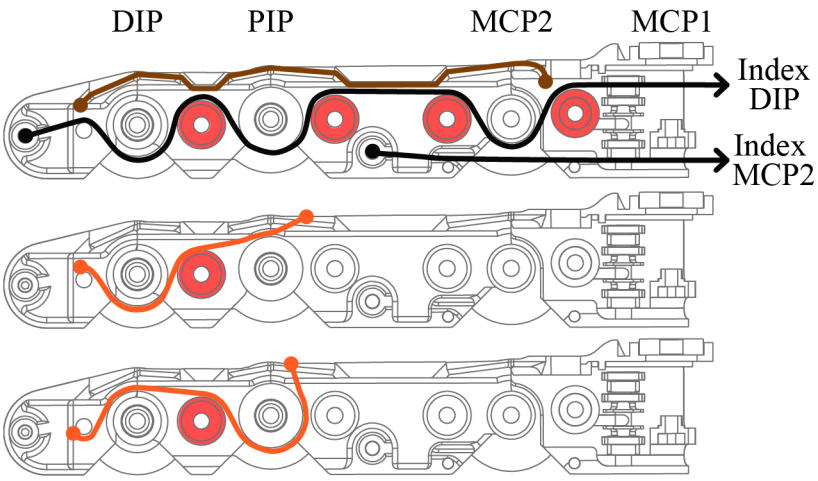

Figure 4.7: Frontal section view of index and middle finger shows tendon routing.

design of index finger (Section 4.3.2), we can formulate the relation between $\dot{\boldsymbol{x}}$ and $\dot{\boldsymbol{q}}$ as follows,

$$\begin{aligned} \dot{\boldsymbol{x}} &= J\dot{\boldsymbol{q}} \\ &= \begin{pmatrix} r_{\mathrm{a1}} & r_{\mathrm{a1}} & r_{\mathrm{a1}} \\ r_{\mathrm{p1}} & -r_{\mathrm{p2}} & -r_{\mathrm{p2}} \\ -r_{\mathrm{p2}} & r_{\mathrm{p1}} & -r_{\mathrm{p2}} \\ -r_{\mathrm{p2}} & -r_{\mathrm{p2}} & r_{\mathrm{p1}} \\ -r_{\mathrm{p3}} & 0 & 0 \\ 0 & -r_{\mathrm{p3}} & 0 \\ 0 & 0 & -r_{\mathrm{p3}} \end{pmatrix} \dot{\boldsymbol{q}} \end{aligned} \tag{4.6}$$

where,

$$\dot{\boldsymbol{x}} = (\dot{x}_{\text{Index DIP}},\ \dot{x}_{\mathrm{c1}},\ \dot{x}_{\mathrm{c2}},\ \dot{x}_{\mathrm{c3}},\ \dot{x}_{\mathrm{e1}},\ \dot{x}_{\mathrm{e2}},\ \dot{x}_{\mathrm{e3}})^T \tag{4.7}$$

$$\dot{\boldsymbol{q}} = (q_{\mathrm{DIP}},\ q_{\mathrm{PIP}},\ q_{\mathrm{MCP2}})^T \tag{4.8}$$

and J is the Jacobian matrix of this specific tendon routing. After that, we apply the conversion on pulley system to exclude the tendons with winding. The new tendon routings is shown in Figure 4.9. Idler pulleys are painted in red.

Figure 4.10 shows four section views of the little finger where the first

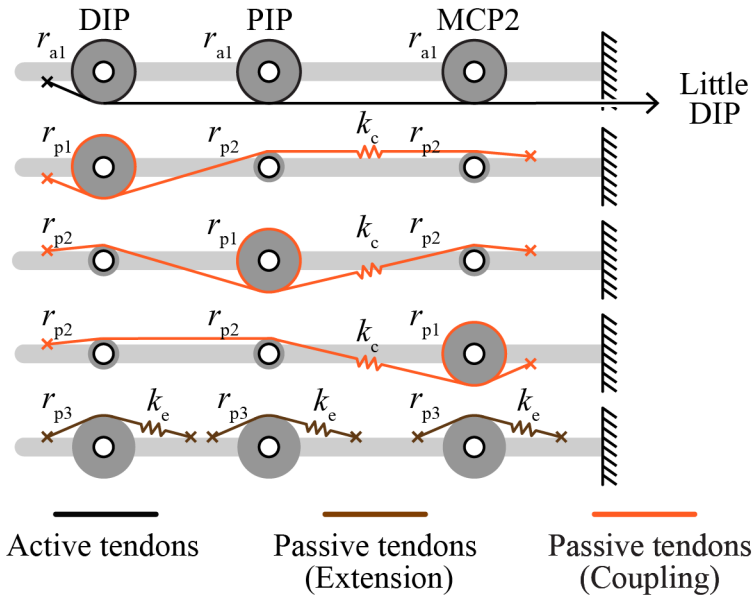

Figure 4.8: Tendon routing of little and ring finger.

layer is the location for an active tendon and extension elastic bands. Again, one brown tendon is routed through the structure but actually it represents three independent passive tendons x_{e1}, x_{e2}, and x_{e1}. The second to fourth layers are area for coupling passive tendons, drawn in orange lines. The design for MCP1 joint is included in the next Section 4.3.5.

4.3.4 Thumb

Thumb, unlike any other fingers, need to move oppose the other four fingers. Consequently, the thumb has to be stronger and more precise in movements. We designed thumb with fully-actuated tendon-driven mechanism. By using our simplified model of the human hand, thumb has 3 joints (TM, MCP, and IP) with 4 DOFs. TM is a 2-DOF joint located at the root of the thumb. To implement 2-DOF joint, we separate it into TM1 and TM2 in adduction and flexion plane respectively. To satisfy limited actuation strokes of actuators, we specify the range of movement in Table 4.3 where it is still enough for the thumb to oppose all other fingers. TM2 joint has around $-10°$ degrees of hyper extension to allow wider space of object caging.

To produce a proper orientation of contact surface of the thumb when opposing with other fingers, axis of joint rotation cannot be parallel. They

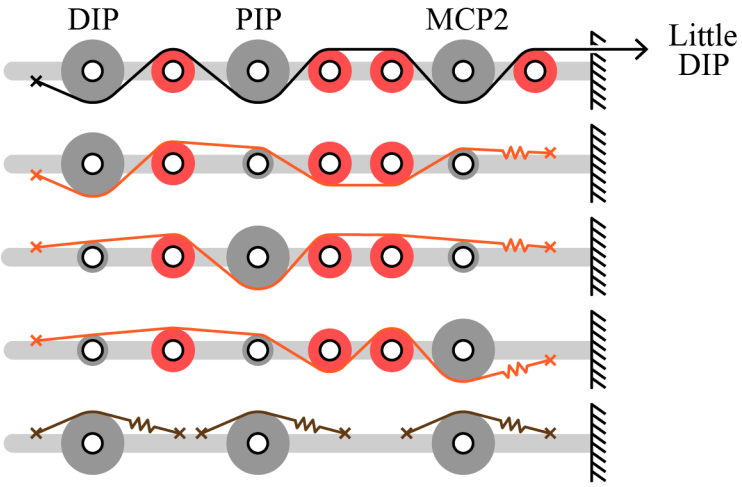

Figure 4.9: Tendon routing of little and ring finger without winding.

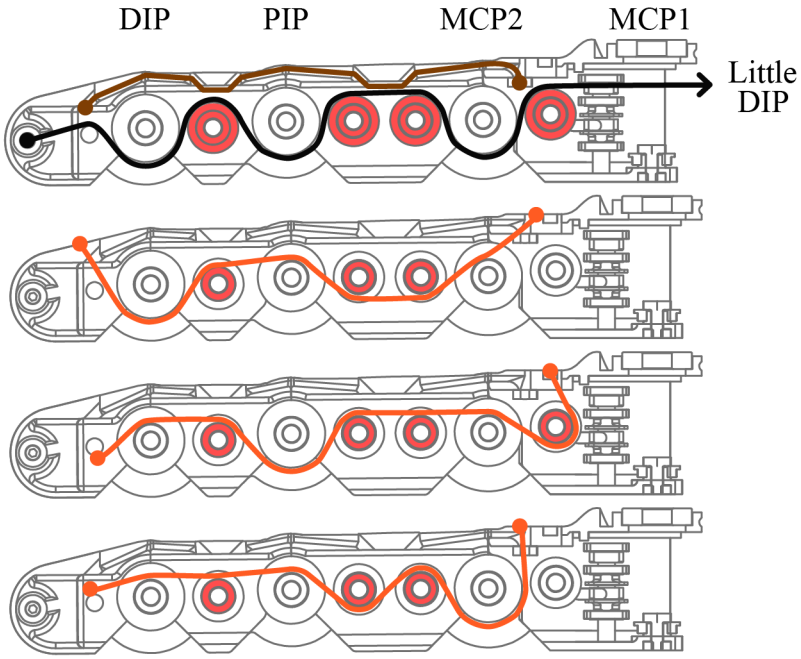

Figure 4.10: Frontal section view of little and ring finger shows tendon routing.

Table 4.3: Movement ranges of the thumb.

Finger	IP	MCP	TM2	TM1
Thumb	0° to 80°	0° to 70°	−10° to 70°	0° to 60°

are inclined as depicted in Figure 4.11. In addition, the first phalanx of the thumb (Metacarpal bone in human) is rotated 45° degree with respect to the first phalanx of index finger (Metacarpal bone) to improve an opposition of thumb.

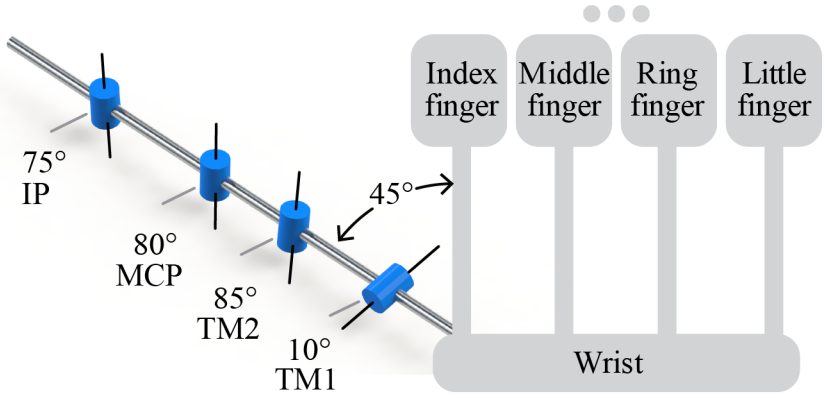

Figure 4.11: Joint configurations of the the thumb.

By using N+1 tendon-driven mechanism, it is possible to perform torque control independently on each joints. As a result, five active tendons are necessary for four-joint finger. We use an optimization routine in Section 2.3.2 to choose the tendon routing that has as uniform as possible the bias forces. We add the following constrains to the optimization to get the practical result for later mechanical design of the thumb.

1. All pulleys has the same radius r_{a1}.
2. There are two active tendons terminated at distal phalanx of the thumb called Thumb IP1 and Thumb IP2.
3. One tendon is terminated on the distal phalanx of MCP joint called Thumb MCP.
4. One tendon is terminated on the distal phalanx of TM2 joint called Thumb TM2.

5. One tendon is terminated on the distal phalanx of TM1 joint called Thumb TM1.

The result of the optimization on tendon routing is shown in Figure 4.12 and and the most uniform for bias is shown in equation The green blocks represent sliding-contact tendon guides which is unavoidable because of the inclined axis TM1 and TM2.

$$\boldsymbol{f}_{\mathrm{b}} = \begin{pmatrix} 1 \\ 1 \\ 2 \\ 2 \\ 2 \end{pmatrix} \tag{4.9}$$

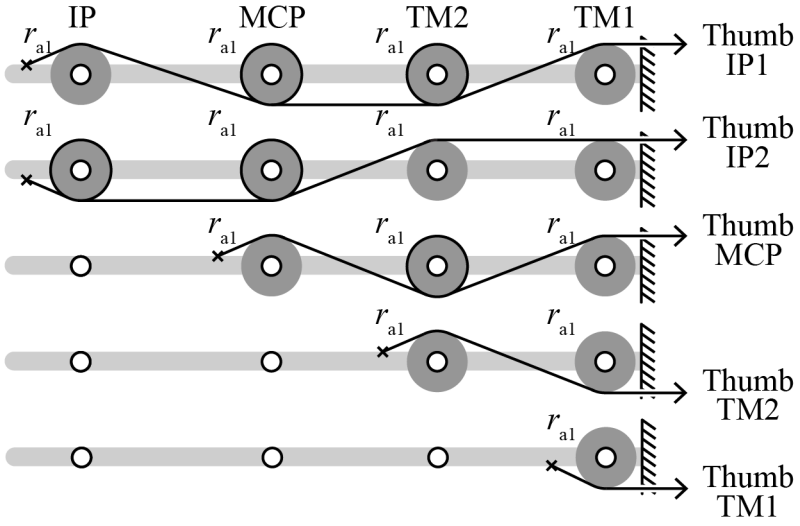

Figure 4.12: Tendon routing inside the thumb.

We can also describe the configurations of tendons with the following equations,

$$
\begin{aligned}
\dot{\boldsymbol{x}} &= J\dot{\boldsymbol{q}} \\
&= \begin{pmatrix}
-r_{\mathrm{a1}} & r_{\mathrm{a1}} & r_{\mathrm{a1}} & -r_{\mathrm{a1}} \\
r_{\mathrm{a1}} & r_{\mathrm{a1}} & -r_{\mathrm{a1}} & -r_{\mathrm{a1}} \\
0 & -r_{\mathrm{a1}} & r_{\mathrm{a1}} & -r_{\mathrm{a1}} \\
0 & 0 & -r_{\mathrm{a1}} & r_{\mathrm{a1}} \\
0 & 0 & 0 & r_{\mathrm{a1}}
\end{pmatrix} \dot{\boldsymbol{q}}
\end{aligned}
\tag{4.10}
$$

where,

$$
\dot{\boldsymbol{x}} = (\dot{x}_{\text{Thumb IP1}},\ \dot{x}_{\text{Thumb IP2}},\ \dot{x}_{\text{Thumb MCP}},\ \dot{x}_{\text{Thumb TM2}},\ \dot{x}_{\text{Thumb TM1}})^T \tag{4.11}
$$

$$
\dot{\boldsymbol{q}} = (q_{\mathrm{IP}},\ q_{\mathrm{MCP}},\ q_{\mathrm{TM2}},\ q_{\mathrm{TM1}})^T \tag{4.12}
$$

and J is the Jacobian matrix of this specific tendon routing of the thumb. The tendon routing shown here is one of the candidate result of tendon-routing optimization, previously described in Section 3.5. Self collisions of tendons due to winding can be reduced by adding idler pulleys to the design. Figure 4.13 highlights the uses of idlers pulley in tendon routing of the thumb.

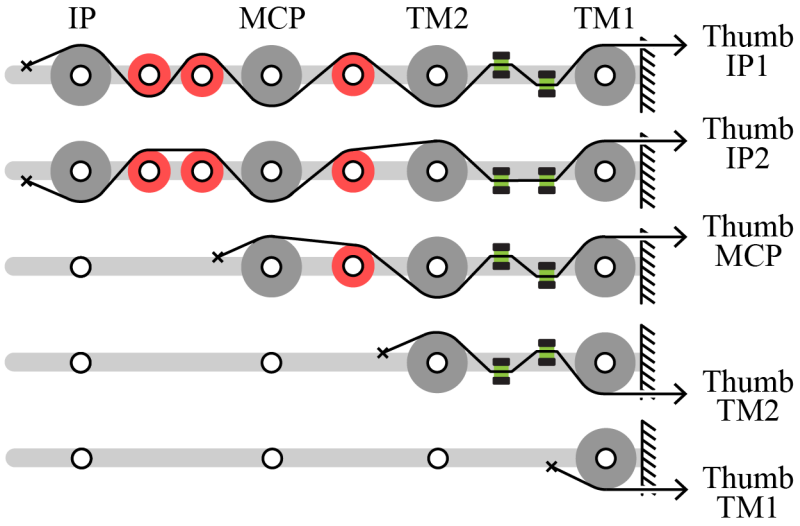

Figure 4.13: Tendon routing inside the thumb with no winding and sliding contacts.

Figure 4.14 is the section view of thumb in frontal plane depicts the tendon routings inside the thumb. Red pulleys are idler ones and the green rectangles are the sliding-contact tendon guides. Another section view of the thumb on saggital plane is shown in Figure 4.15. Sliding-contact tendon guides also make the routing simple and much smaller so that TM1 and TM2 joint can be placed close to each other.

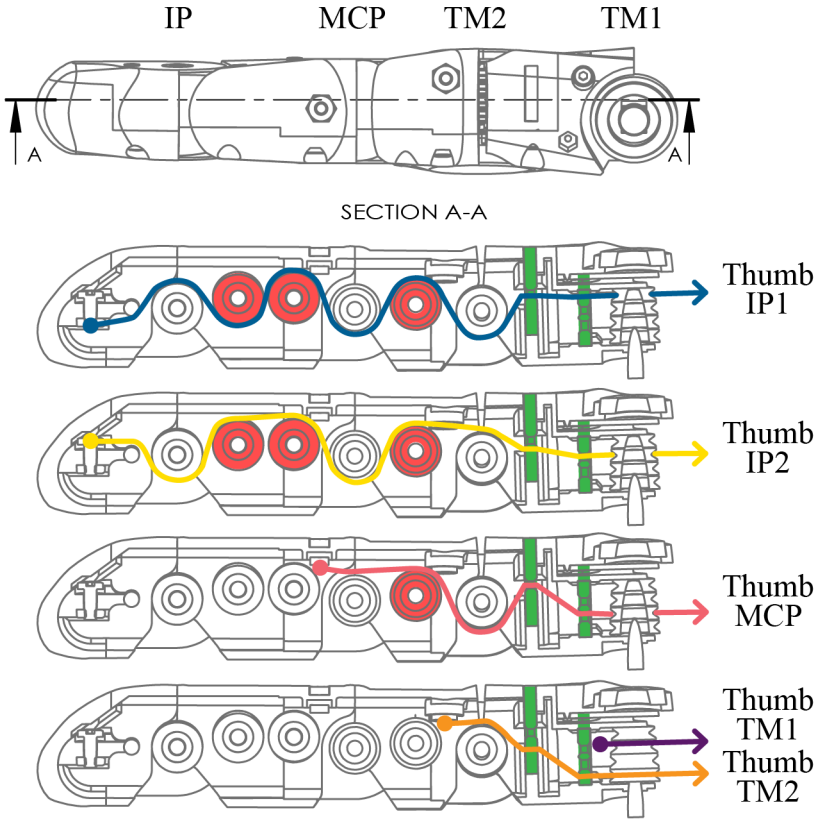

Figure 4.14: Frontal section view of the thumb shows tendon routings inside.

4.3.5 Palm

In our simplify model, originally there is no explicit movement in the palm but since we separate MCP joint into MCP1 and MCP2, we consider MCP1 joints as the part of the palm while MCP2 joints are located in fingers. It would be costly if we actuate four MCP1 joints of index, middle, ring, and little fingers independently. Therefore, MCP1 joints of all four fingers are

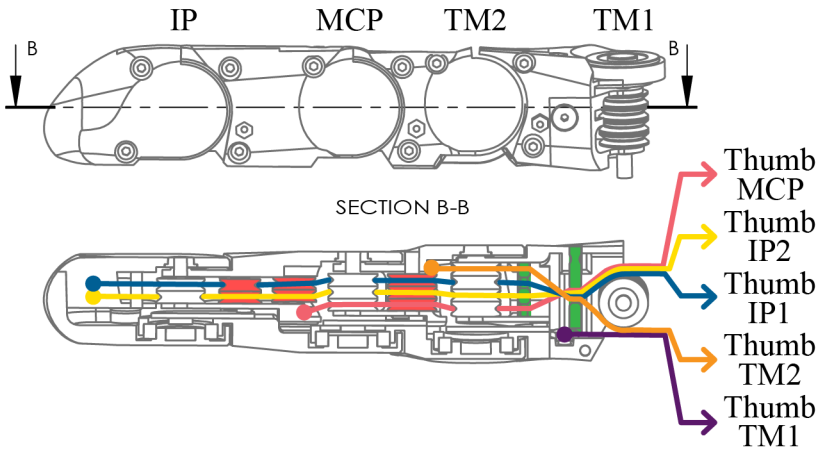

Figure 4.15: Sagittal section view of the thumb shows tendon routings inside.

design with underactuation. Abduction and adduction movement can be seen as coordination movements, for example, four fingers abduct or adduct at the same time.

The mechanism for adduction and abduction movement is shown in Figure 4.16. The middle finger is fixed with respect to the palm to provide the center of abduction and adduction. Blue lines represent compression springs which produce the separation forces between fingers, resulting in abduction movement. Adduction motion is controlled by one active tendon, denoted by Adduction.

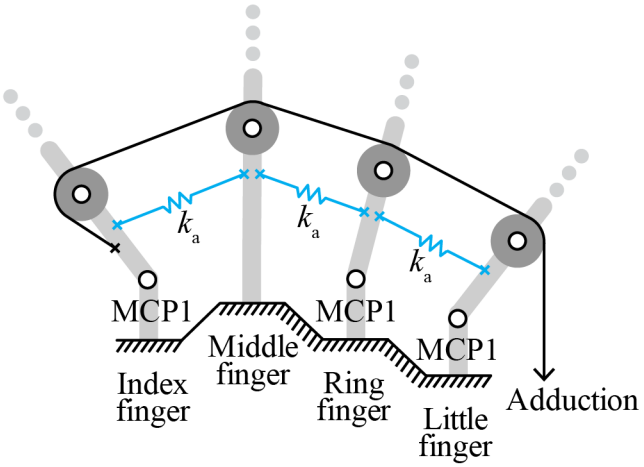

Figure 4.16: Abduction mechanism implemented by compression springs.

To implement abduction and adduction mechanism, we propose to use elastic band instead of spring due the requirement of spaces. However, the behaviour of elastic bands is not the same as compression spring because elastic bands produce tension forces which is opposite to the compression forces created by springs. Hence, the placement of springs need to be reconsidered and the result is shown in Figure 4.17.

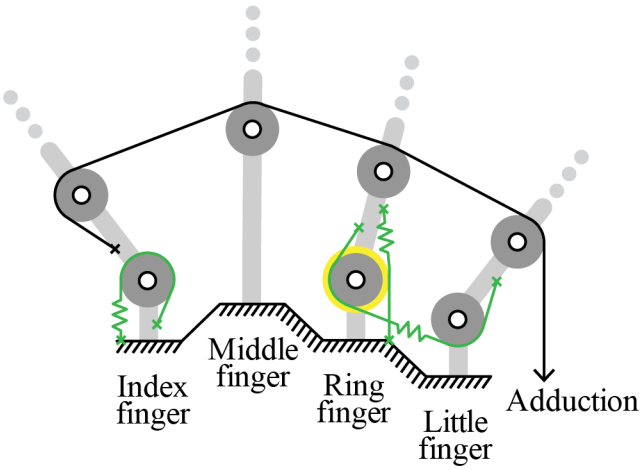

Figure 4.17: Abduction mechanism implemented by elastic bands.

Figure 4.18 suggests the saggital plane section view of the abduction mechanism where axis of MCP1 are shown in yellow dots and idler pulleys are painted in red. The only adduction active tendon is the black line. Three green lines are the routing of elastic bands along the grooves. To keep moment arms created by green elastic bands as constant as possible, the outer curvature of the components that have contacts with passive tendon are designed to be circular chord where the center is located at MCP1 joints (yellow dots).

A number of tendons, joints, type of mechanism and type of coupling are summarized in the Table 4.4. Besides abduction and adduction mechanism, palm is also the area where all the active tendons, twelve in total, from fingers are guided before entering the wrist and ending at linear actuators. By reducing the number of sliding contacts as much as possible, we route the tendons with idler pulleys. The concept is introduced already in Section 3.3. We model all the connections of tendons by using 3D sketch in Computer-aided design (CAD) software.

Figure 4.18: Saggital section view of the palm shows abduction and adduction mechanism.

Table 4.4: Number of tendons, joints and mechanism on each finger.

Fingers	Tendons	Joints	Mechanism	Coupling
Thumb	5	4	Fully-actuated N+1	
Index	2	4	Underactuated	DIP/PIP
Middle	2	4	Underactuated	DIP/PIP
Ring	1	4	Underactuated	DIP/PIP/MCP2
Little	1	4	Underactuated	DIP/PIP/MCP2
(Adduction)	1	3	Underactuated	3 × MCP1
Total	12	19		

The routing of tendons has to satisfy following property. First, the number of pulleys required to change tendons from one configuration (direction and location) to the others has to be minimized. In our proposed design, we are trying use only 2 pulleys for each tendon which actually the minimum pulleys. Second, the routing must be collision free. Next, all tendons have to be in parallel before escaping the palm which simplify the design of the wrist. Finally, we build a structure that support the pulley systems under the constraints that all the holes that support pulleys' shafts have to be accessible from out side because it has to be machined to get the precise fitting and assembly afterwards. Figure 4.19 depicts one possible solution of tendon routing that satisfy previously mentioned criteria. The figure is

drawn with right angle projection where the top left is top view look from the back side of the right hand. White pulleys are the pulleys that oriented in 3-dimensional space. Due to the very limited space, two tendons (Little DIP and Adduction) cannot be routed by pulleys. Therefore, they are guided with low friction plastic bushes, drawn in black. Still the tendons' bending angles for those two tendons are minimized by the location of bushes to reduce a friction due to sliding contacts as much as possible.

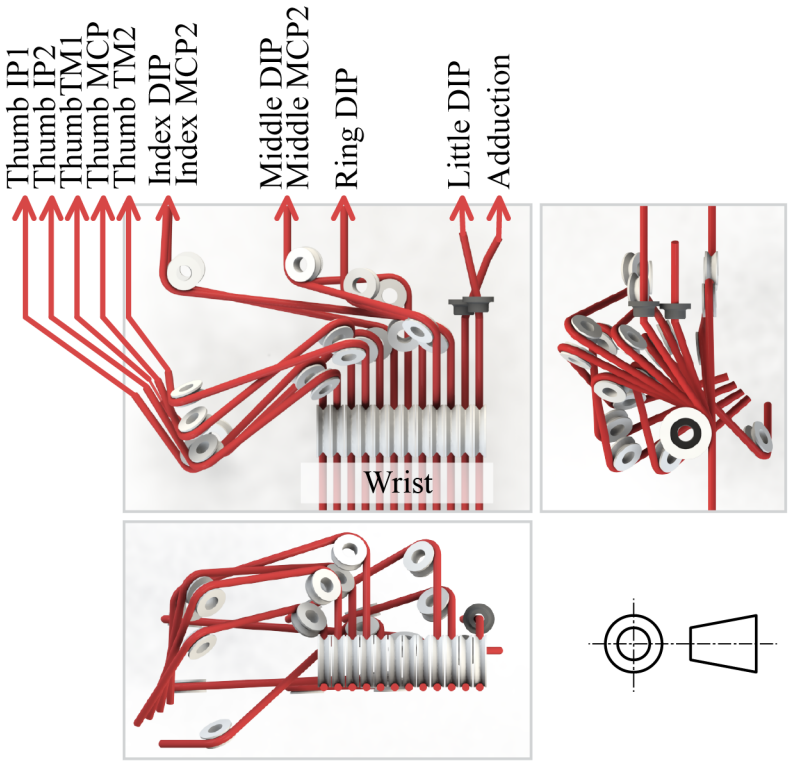

Figure 4.19: Tendon routing in 3D space inside the palm, shown in third angle projection.

After we get the 3D sketch of tendon routing, we model the structure that supports those pulley systems by projecting minimal support structure of each pulley onto the fixture plane. Figure 4.20 shows the tendons in red with the support structures in yellow. According to our design criteria, all the shafts' holes and slots for pulleys are accessible from outside to be able to machined them afterwards. There are clearance holes for every entrances and exits of tendons to prevent tendons from derailing even in the case of

no tension applied on tendons.

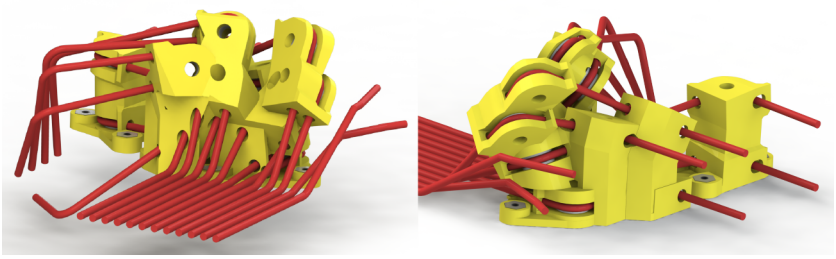

Figure 4.20: Three-dimensional structure that supports pulley inside the palm.

The pulley support structures are assembled inside the palm, see Figure 4.21. For ease of assembly palm is divided into two parts; main structure and top cover. The main structure of the palm is shown in green which is almost the pulley-support structure of some tendons from the thumb. By can be seen clearly that all the tendons that exit the palm are parallel.

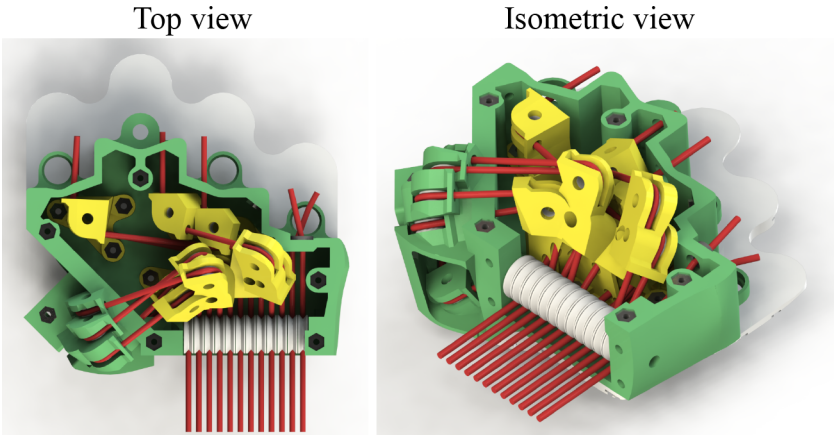

Figure 4.21: The main structure of the palm with pulley-support structures inside.

Top cover of the palm is designed to mimic the curvature on the back side of human hand while is the same time it is the smallest cover that enclose all the components inside, shown in figure 4.22. There is another small cover, light-green, is another small cover over the top cover. Between those two covers, it is a location for signal cables' connectors (more details are described in Section 4.4.4.

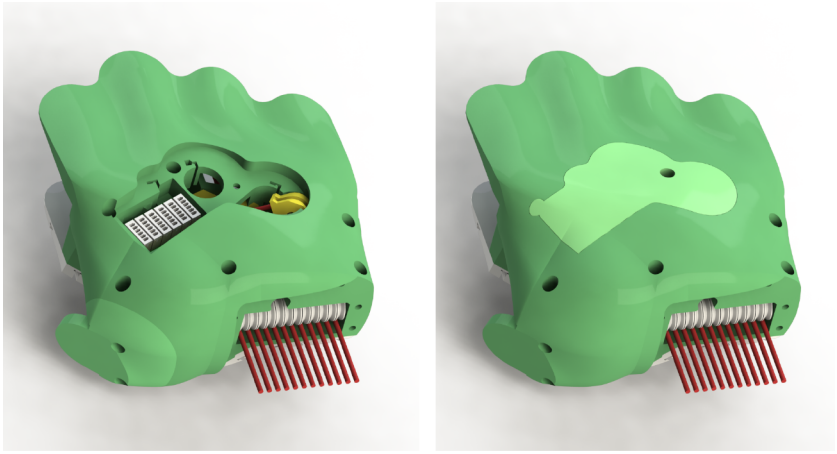

Figure 4.22: Top cover of the palm where curvature are inspired by that in human.

The bottom side of the palm is covered with another plastic component to mimic the curvature of human palm, illustrated in Figure 4.23. Since a palm surface also has a contact with objects during grasping, the bottom surface is then made with silicone to increase the contact frictions. Silicone parts are deformable which also benefit in increasing the grip. To implement, the silicone surface we first made the bottom sureface of the palm with ABS plastic, shown in white, and then the inverse of bottom surface with offset distance are made, green component in Figure 4.24, which will be used as a casting mold. By using insert casting technique we can build the silicone surface over the plastic component.

4.3.6 Wrist

Wrist is a connection between hand and forearm in human where in the case of our design, wrist is a necessary component to fix the hand with respect to the actuators. Humans' wrists have around 3 DOFs. By counting 3-DOF shoulder and 1-DOF elbow joint, human arm has 7 DOFs which resulting in having a redundancy in joint space that help expanding the end effector task spaces. However, to simplify the design of wrist, we propose to fix the wrist with respect to forearm while most of the components must be reusable even in the case of adding few-DOF wrist in the future.

Since the main function of the wrist is to connect tendons from a hand

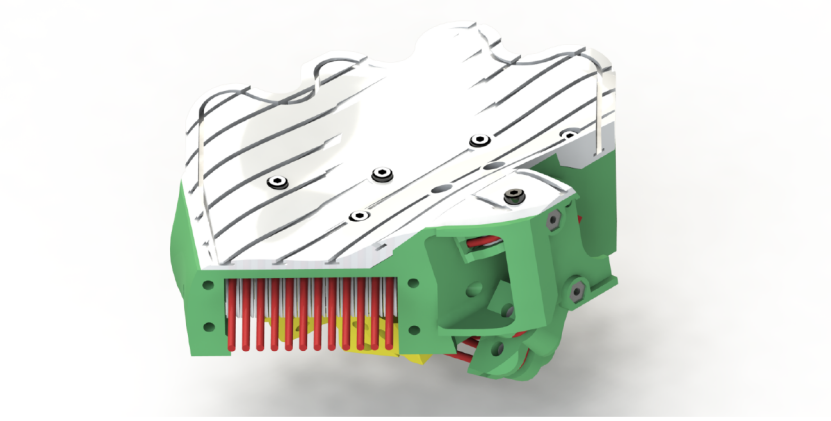

Figure 4.23: The buttom surface of the palm that mimic curvature of human palm.

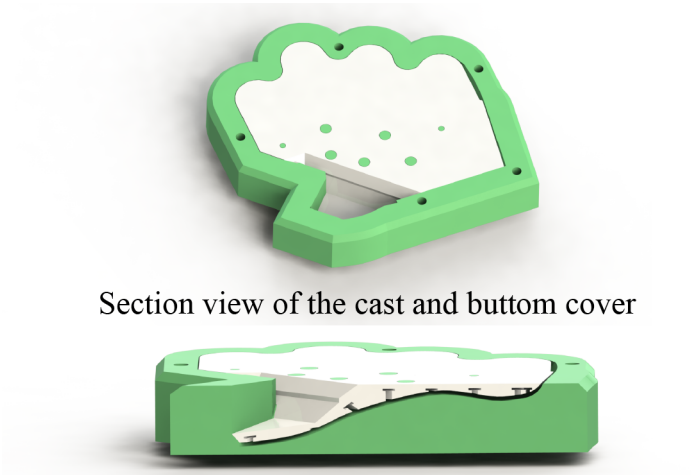

Figure 4.24: Buttom cover of the palm and its insert molding cast.

and guide them to linear actuators. One possible solution to change the direction of tendons is to design a pulley system oriented in 3D space. By doing so, we use the similar technique as what we did for the palm in Section 4.3.5. Figure 4.25 show the pulley support structure as a result of designing tendon-routing with collision free. To save the actuator spaces, we arrange 12 actuators into 3 layers with at most 5 actuators on each layer. Figure 4.26 is the wrist looking from backside of the hand. It can be seen that all tendons on actuator side are parallel, as well as the tendons on the hand side.

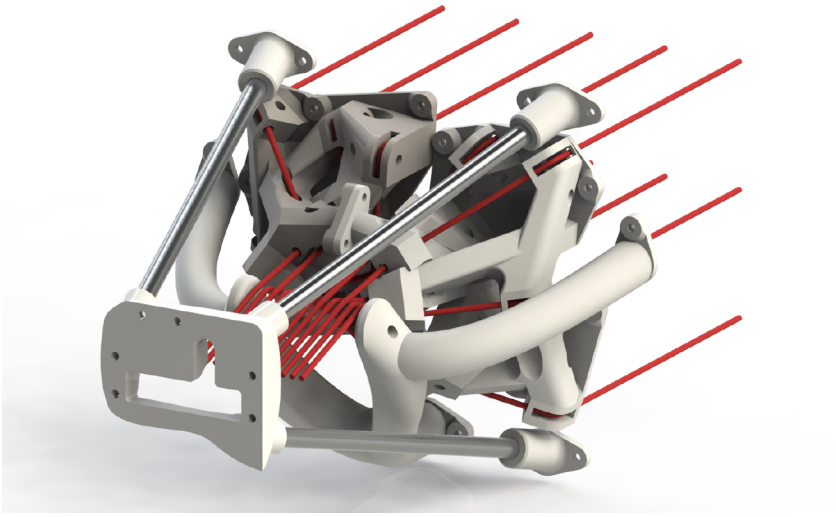

Figure 4.25: Isometric view of the wrist that has no DOF.

4.4 Sensors and Circuit Designs

Though we can measure the displacements of the actuators but still they are not enough to determine the joint space configuration of the underactuated hand. Most of the designs were not included the joint angle sensors because of the limitation in space and handling the signal cables is another big issues. One common type of joint sensors is potentiometer [12]. However, the analog output signal is not robust against the noise and it requires one signal cable per one joint which seems to be small but considering 20-DOFs hand, at least 20 cables are needed. To overcome those problems, we proposed to use the sensors with digital output and serial capability.

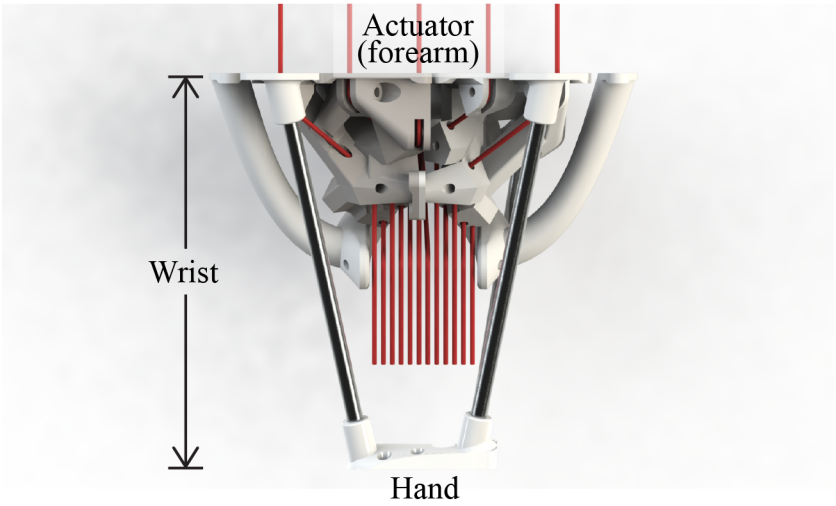

Figure 4.26: Top view of the wrist looking from backside of the hand.

In this section, we will go through the design of joint angle sensors. We begin with the choices of magnetic encoders and then we review the structure of fingers that enables the use of them. By using the serial communication protocol of the magnetic encoders, we can reduce the number of signal cables. Later, the designs of circuit boards are presented and finally, the routing of signal cables are discussed.

4.4.1 Magnetic Encoders

There are two types of magnetic encoders, incremental and absolute. The incremental one needs always on connection between sensors and microcontroller which is not the case of absolute one. An absolute magnetic encoder is available only for the on axis measurement, see Figure 4.27. The chip (below) measure the absolute position of the magnet's rotation angle by using Hall sensors inside.

The main difficulty of using on-axis measurement magnetic encoder is that the magnet has to be located in-line with the rotational joint's shaft. We solve that problem by designing finger joints with two-separate bearings supported by the outer structure where magnets and sensors are fixed inside the structure. Figure 4.28 shows the saggital section view of PIP joint. There are two bearings that support the rotational joint, painted in yellow. One bearing has a diameter large enough to contain the magnet inside, in flavour

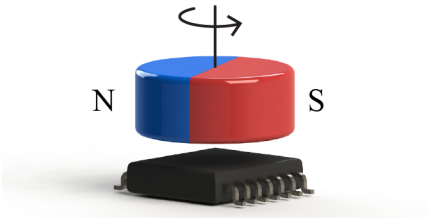

Figure 4.27: On-axis angle measurement of absolute magnetic encoder.

of making the fingers thinner.

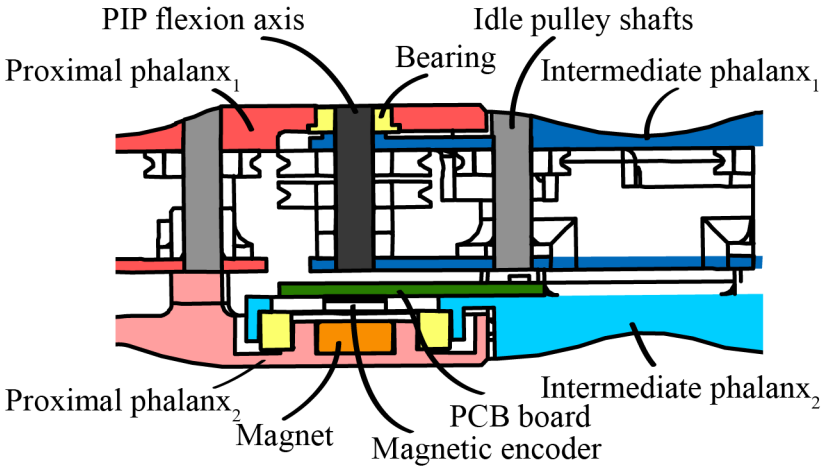

Figure 4.28: Joint structure that enables an integration of encoder inside.

4.4.2 SPI-Daisy-Chain Communication

The absolute type magnetic encoder AS5048A from Austriamicrosystems (AMS) is chosen for the implementation of joint encoders. The chip itself integrates the Serial Peripheral Interface bus (SPI). SPI is a communication through 4 digital signals: CLK for clock, $\overline{CS}$ for falling edge triggered chip select, $MOSI$ for master input slave output and $MISO$ for master output slave input. For a hand with 19 joints, CLK, $MOSI$, and $MISO$ can be shared among all sensors while each sensor has its own $\overline{CS}$ to enable reading or writing sensor by sensor. In total it requires at least 22 signal cables which is still a large number.

To reduce the number of signal cable furthermore, we use SPI on the

other configuration called daisy chain. SPI-daisy-chain can be done by connect $MISO$ of one sensor to the next sensor's $MOSI$. By doing so the data previous sensor in the chain is forwarded to the next component. Figure 4.29 shows the connect of signal cables between all component in daisy chain mode. As a result, no matter how long the chain is only 4 signal cables are necessary for the communication.

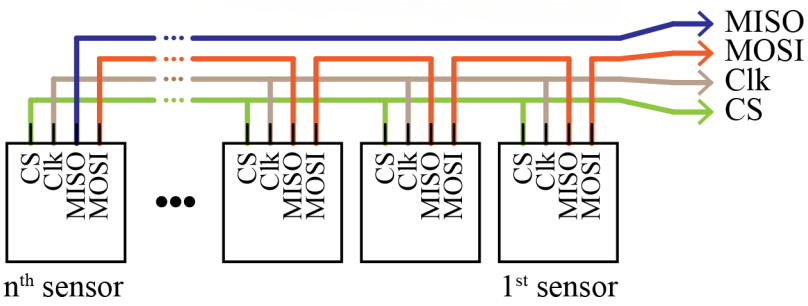

Figure 4.29: SPI daisy-chain communication on n sensors.

The timing diagram for SPI daisy-chain is shown in Figure 4.30. In this example, we transmitted and received data over 4 sensors by using only 4 signal cables: CLK for clock, $\overline{CS}$ for falling edge triggered chip select, $MOSI$ for master input slave output and $MISO$ for master output slave input. The communication begin with transmitting read command through MOSI for 4 sensors (C1, C2, C3 and C4). After that 4 sets of data from each serially-connected sensor are replied back to the host microcontroller. To avoid losing the sensor data due to lower sampling frequency in daisy-chain mode, the SPI clock frequency has to be selected carefully. The theoretical data sampling frequency of SPI daisy chain with n sensors in the chain can be expressed as followings,

$$f_{\text{sampling}} = \frac{f_{\text{CLK}}}{2 \times n \times b} \tag{4.13}$$

where b is the number of bit of each read packet, f_{sampling} is the data sampling frequency of the daisy chain, and f_{CLK} is the SPI clock frequency. Sampling frequency is divided by two because we consider b-bit transmission and b-bit reception of every single sensors. In our implementation AS5048A magnetic encoder has 16-bit packet size and if we connect 19 sensors in the single daisy chain running SPI clock at 4 Mhz, we would get data sampling

frequency around 6.53 kHz or data comes every 153 microseconds which is still fast enough for the basic position control.

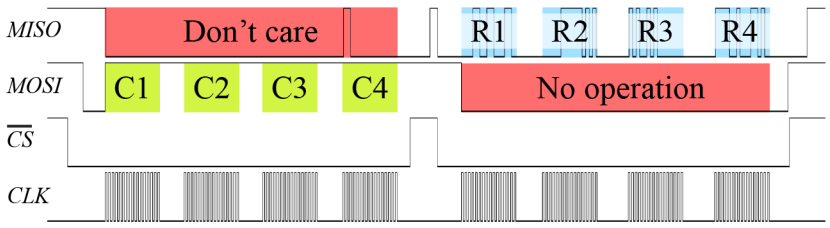

Figure 4.30: Timing diagram shows how communicate with SPI daisy-chaining sensors.

4.4.3 Circuit Designs

The circuit board for each magnetic encoder has to fit inside every joints of the finger. To reduce the number of distinct designs, we try to reuse the same design of circuit board but since spaces inside the fingers are very small, it is not possible to use any means of connector to connect between board. The only choice we have is to solder the wires directly on to the board. Thin wires are preferred over the flexible printed circuit board (FPCB) because they can be bended in any direction while FPCB cannot be bended in the surface plane. The more number of soldering connection, the higher possibility of broken. Therefore, we propose to reduce the number of connections designing the circuit board that combines sensors on the same phalanges. Figure 4.31 depicts three types of the circuit boards. The top one contains only one encoder and they are used on the thumb and DIP, MCP1 joints of the index, middle, ring and little finger. The sensor board on the second and third rows has 2 encoders for MCP2 and PIP joints. They have different size correspond to the length of the proximal phalanges of index finger (middle and ring finger as well) and little finger.

4.4.4 Routing of Signal Cables

One important point of our proposed robot hand design is that, it includes all sensors and signal cables inside the structure. In this section, we will present how the cables are connected in the fingers as well as in the palm.

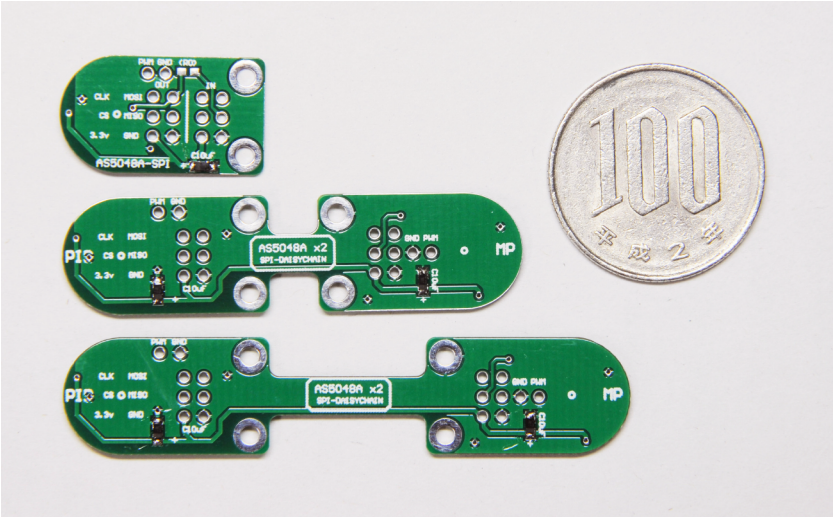

Figure 4.31: Three designs of the sensors' circuit boards.

4.4.4.1 Fingers

Each phalanx of the fingers is composed of two main components separating along the longitudinal plane of the finger. The first component contain tendons and pulley systems for an actuation while the other component enclose magnetic encoders and circuit boards. Figure 5.25 highlights a set of components that contain circuit boards. There are 6 wires, 4 digital signals and 2 powers, connecting all the sensors in SPI daisy chain manner. The above figure shows the cables inside index finger (as well as middle and ring finger) while the lower one shows the same for little finger. Cables exit the internal structure of the finger through a small hole on metacarpal phalanges.

4.4.4.2 Palm

Palm, in our design not only the center of actuation tendons, is also the place where all SPI daisy chain from each single finger connects together and at the end only 6 cables connect them to a microcontroller. We design tracks for cables inside the palm. Figure 4.33 show the routing diagram of all signal cables. Each line in the diagram actually contains 6 signal cables. The blue lines are cables enclosed inside the finger structure, discussed in Section 4.4.4.1. After cables escape Metacarpal phalanges, they go through

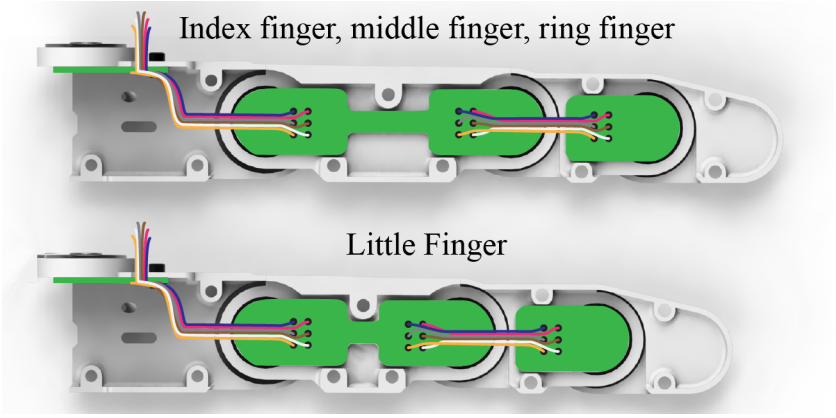

Figure 4.32: Routing of signal cables inside index and little finger.

small holes to enter internal structure of the palm, drawn in pink. Then, 5 red cables from each finger daisy chain connect each other with small connectors over the top cover of the palm (Figure 4.22). Finally, yellow cables are the output that connects to a microcontroller.

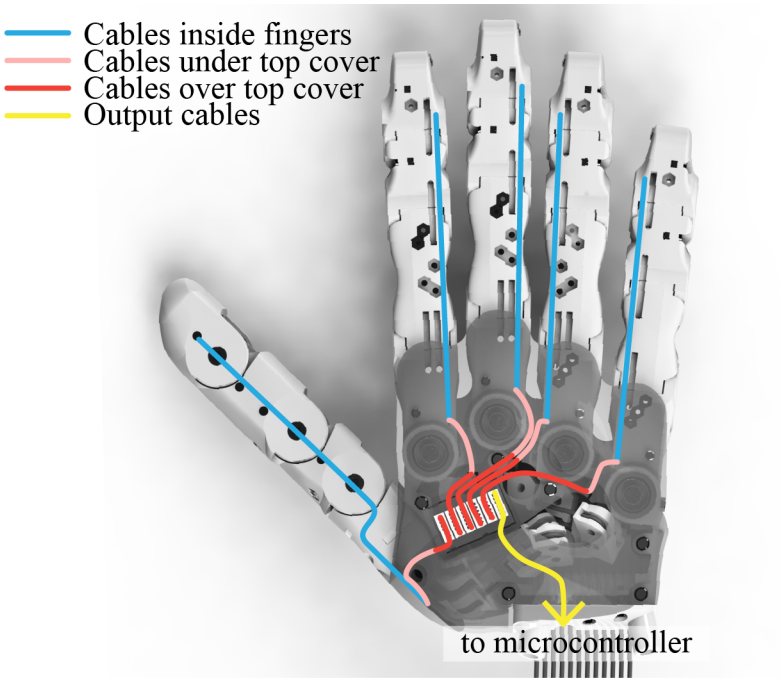

Figure 4.33: Routing of signal cables inside the palm.

Chapter 5

Hand Prototype and Experiments

5.1 Introduction

By using rapid prototyping as a fabrication process, we build the prototype hand which is shown in this section. We also discuss about the experiments on tendon termination. The hand prototype is assembled and demonstrations on the movement of the hand is shown in experiment section. Finally, we exploit our hand design that include joint angles sensors to do the movement analysis of index and little finger.

5.2 Rapid Prototyping Process

Rapid prototyping technologies enable designers to build a fast prototype. We choose 3D-printing process because the prototype can be done very fast and cheap compared to other techniques. Products are made of ABS plastic which has good impact resistance and toughness. In this section, we will explain how we use 3D-printing process to build the final products. Starting with some detail about the 3D-printer that we are using. Later, we introduce the epoxy infiltration process to increase the overall strength of 3D-printed parts.

5.2.1 Dimension SST 1200: Rapid Prototyping Machine

Dimension SST 1200 is a 3D printer based on Fused Deposition Modeling (FDM) process [24]. In order to build any shape product two types of material are necessary. The first type that will be end up as a product is ABS plastic while sometimes where there is an overhang in the design, printed model material (ABS) may fall due to gravity. Therefore, the PLA plastic are printed along with ABS model to form the support structures. After the printing process is over, support material (PLA) is removed by dissolving the product in Sodium Hydroxide solution which reacts only PLA not ABS. Figure 5.1 shows the same part printed by Dimension 3D-printer. The yellow parts are ABS model material while the one in brown is PLA support material. On the left is the part before dissolving in support-removal solution while right one is the same part after supports are removed.

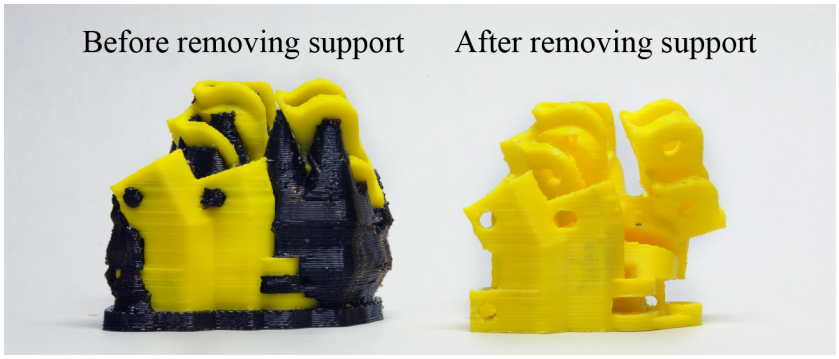

Figure 5.1: Part made by 3D-printing process with support material.

5.2.2 Epoxy Infiltration Process

The main source of the weakness in 3D-printed parts comes from the pores in between the printed layers where ABS plastic does not perfectly fused and becomes a solid piece. We develop an epoxy infiltration process to fill the gaps between layers which results in stronger parts. We chose the low viscosity epoxy from Genus company GM-9002 which is originally intended for detailed casting. After parts are fabricated with 3D-printer and support materials are already removed, we paint an epoxy onto the surface. Right after the painting, part are vacuum in the closed chamber to remove air trapped inside the parts (air trapped in between printed slices). Here, we

can observe that air bubbles appear on the parts' surface and then we release the value to let the air goes inside the chamber that is when infiltration process has begun. We alternate epoxy painting can vacuum process until there is no bubble appears on the surface during vacuum. It takes around one day to let the epoxy fully cured in the constant temperature oven at temperature around 55°C.

5.3 Experiments on Tendon Terminations

When we apply stresses on the tendon with knots, the stresses do not distribute to all the fibres equally due to the bending of tendons in the knots. If the applied stresses is over the ultimate tensile strength of the fibres, some fibres start to worn out and the whole tendons are torn at the end. It is worthwhile to test several knotting techniques and also elongations before they break.

5.3.1 Experiment Setup

To test the maximum strength of knotting techniques, we use 1.5mm diameter Dyneema™tendon from Hamilon Company which the maximum strength is rated around 2865N. For each knotting techniques, including Brummel splice [25], Uniknot [26] and Butline hitch [27], we prepared 3 samples where both ends of a sample has the same type of knot. We add another set of samples where we use multi-purpose epoxy to glue around the Brummel splice. By using Brummel splice as a base line for making tendon-end loop, we also prepare Double fisherman's bend that connects two tendons in the middle which benefits an intermediate connection of tendons.

In addition to the knotting technique, we also vary the tendon termination structure. There are two types of the structure. First, the termination structure with compression force generated by the bolts which results in an increasing friction between tendons and the structure, see Figure 5.2. The other one has on compression force on tendons which is done by making a structure that holds a bolt inserting into the tendons' knot, shown in Figure 5.3.

For each of the termination structure, we change the bolts' size as well. According to the rough calculation on shear strength of stainless steel bolts, the shear strength of M3 is around 1700N while 3000N for M4. On the Figure

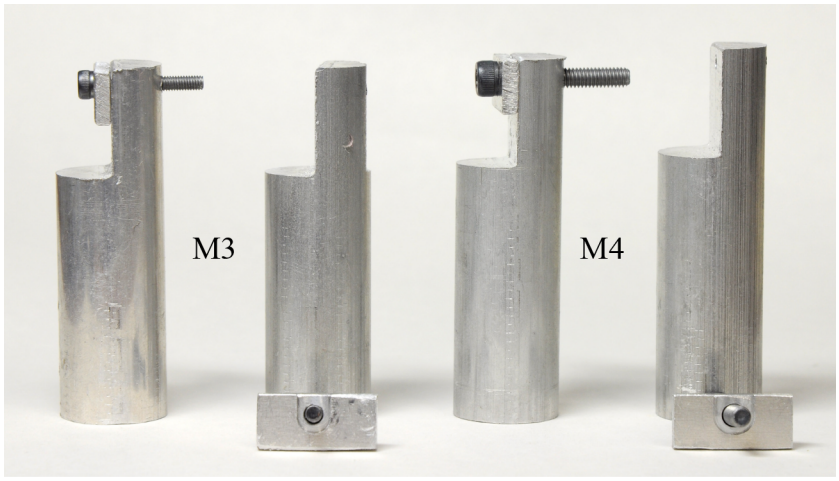

Figure 5.2: Termination structures with compression force.

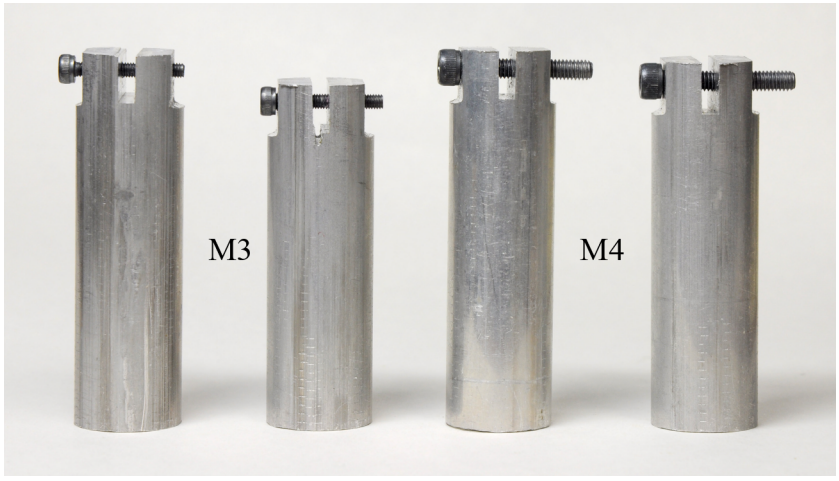

Figure 5.3: Termination structure with no compression force.

5.2 and the Figure 5.3, two rods on the left have M3 bolts while the ones on the right have M4 bolts. Figure 5.4 shows the pulling test configuration. Red lines are the tendon with several knotting technique on both ends. The jigs for tendon termination structure are designed so that tendon lies on the axis of the rod to reduce the bending moments as much as possible.

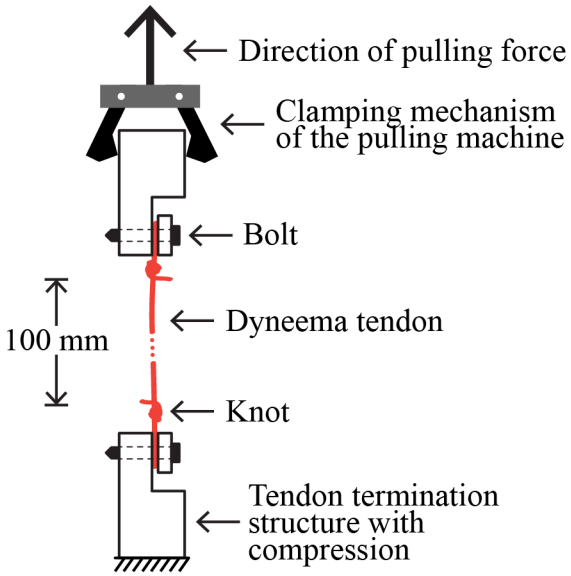

Figure 5.4: Experiment setup on knotting strength test.

To test pulling each sample up to the ultimate tensile strength, we use the universal testing machine which can pull upto 10 tons of force. During the experiment tension forces and elongation of tendons are recorded. Figure 5.5 shows the universal testing machine where samples and jigs are installed in the middle of two clamps.

5.3.2 Results from Pulling Experiments

The pulling experiment is done over 36 samples from 12 combination of knotting techniques and tendon termination structures where each configuration of the test is done over 3 samples. Table 5.1 explains the definition of each test code that covers all the pulling experiments.

The result of each experiment setup are plotted in Figure 5.6 to Figure 5.17. Vertical axis is the tension force and horizontal axis is the tendons' elongation. There are 3 plots on each graph that represent three samples.

Figure 5.5: Universal testing machine.

Table 5.1: Summary of all tendon configurations.

Test code	TTS[1]	Bolt size	Knotting technique	IK[2]	Epoxy
f-b-m3	Compression	M3	Brummel splice	No	No
f-be-m3	Compression	M3	Brummel splice	No	Yes
f-b-m4	Compression	M4	Brummel splice	No	No
f-be-m4	Compression	M4	Brummel splice	No	Yes
f-be-m4-d	Compression	M4	Brummel splice	DF[3]	Yes
f-u-m4	Compression	M4	Uniknot	No	No
f-bh-m4	Compression	M4	Buntline hitch	No	No
s-b-m3	No Compression	M3	Brummel splice	No	No
s-be-m3	No Compression	M3	Brummel splice	No	Yes
s-b-m4	No Compression	M4	Brummel splice	No	No
s-be-m4	No Compression	M4	Brummel splice	No	Yes
s-u-m4	No Compression	M4	Uniknot	No	No

[1] TTS = Tendon Termination Structure
[2] IK = Intermediate Knot
[3] DF = Double Fisherman's bend

The first two samples are pulled from the rest to the breaking point while the third one is pretension up to 1000 N before being released and start pulling until the ultimate tensile stress. The third samples with pretension are denoted by "pre".

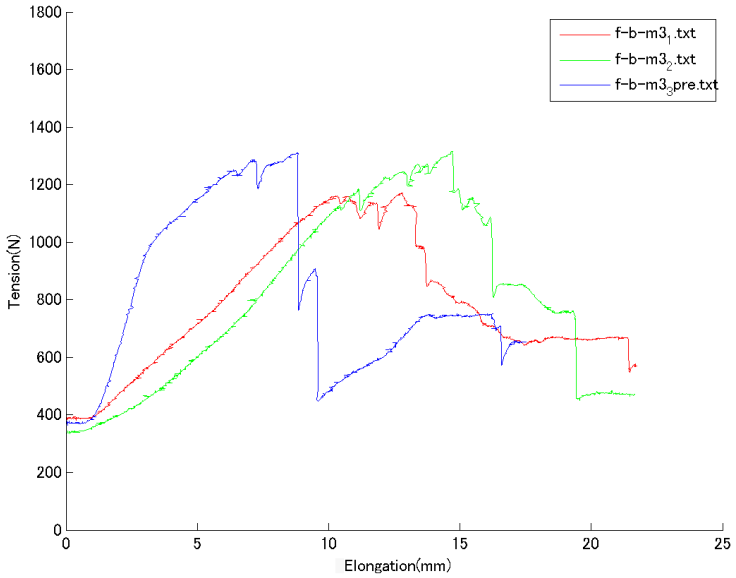

Figure 5.6: Plot of compression-based termination of M3 bolts and Brummel splice

From the graphs, we collect tensions and elongations at the breaking point of each experiment setup and the result from analysis is shown in Table 5.2. From the result, we can summarize the following behaviours of tendon knots in the strength test.

1. Within the same termination structures and same size of bolts, tendons with Brummel splice has relatively higher tension and less elongation at the breaking point when compared to tendons with Uniknot and Buntline hitch.

2. The intermediate connection made with Double fisherman's (f-be-m4-d) bend significantly reduce the maximum tension and also increase the elongation by almost three times compared to ones without (f-be-m4).

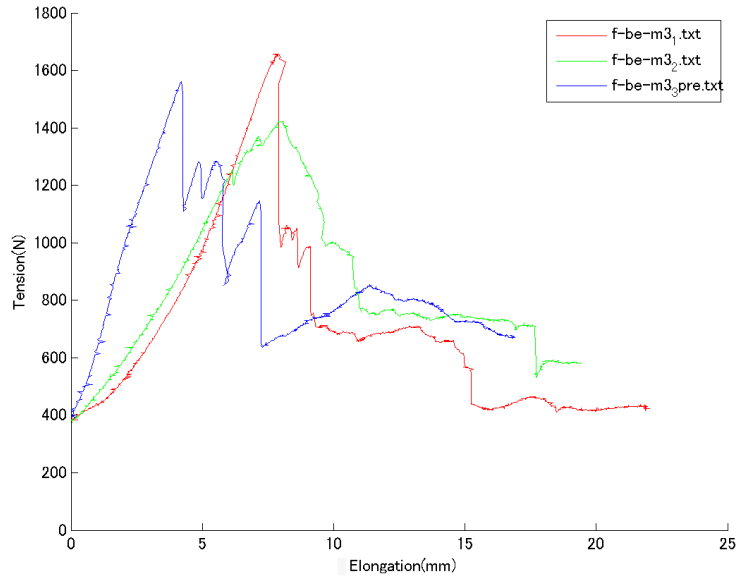

Figure 5.7: Plot of compression-based termination of M3 bolts and Brummel splice with epoxy

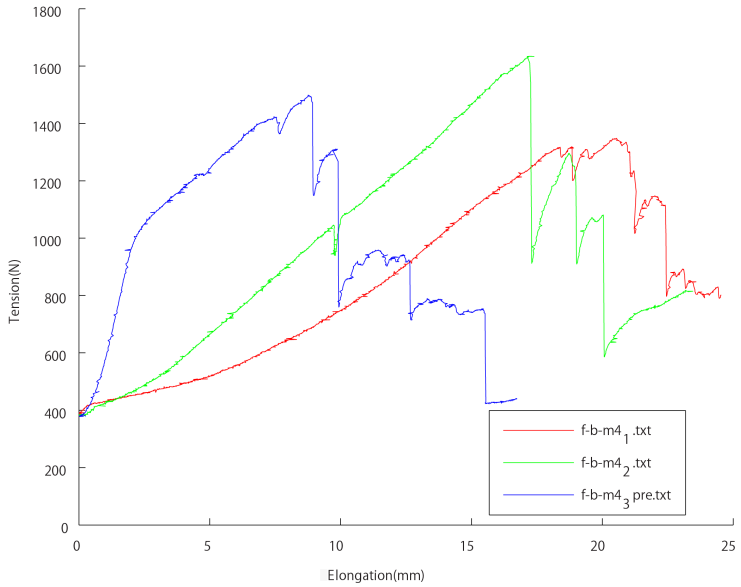

Figure 5.8: Plot of compression-based termination of M4 bolts and Brummel splice

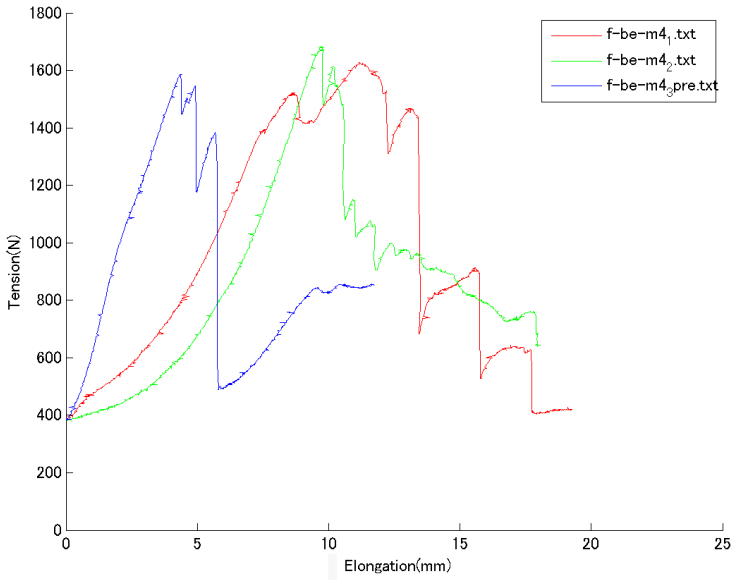

Figure 5.9: Plot of compression-based termination of M4 bolts and Brummel splice with epoxy

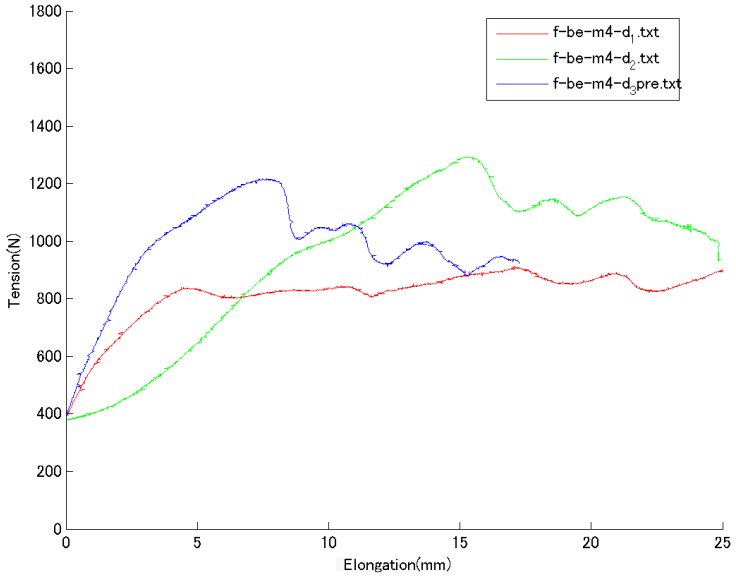

Figure 5.10: Plot of compression-based termination of M4 bolts, Brummel splice and double fisherman's connection

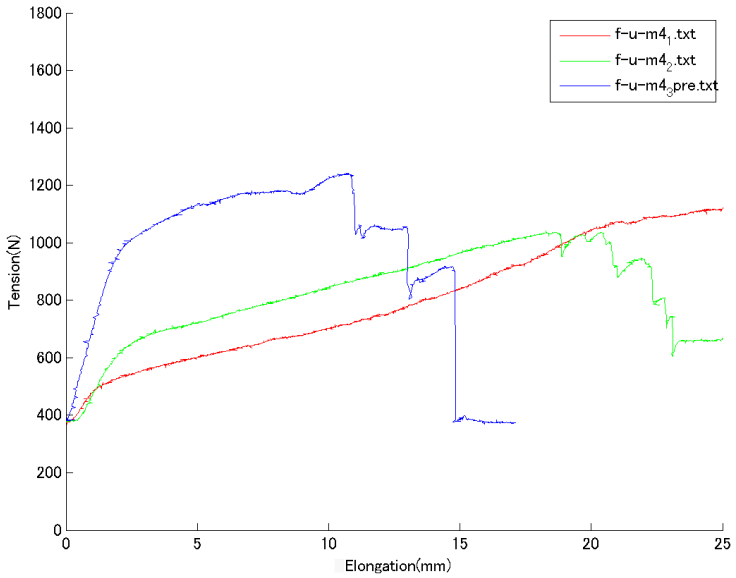

Figure 5.11: Plot of compression-based termination of M4 bolts and Uniknot

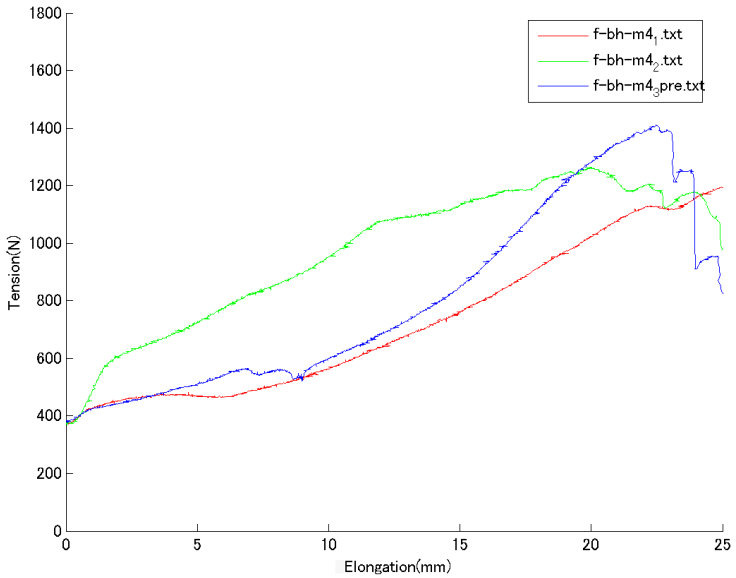

Figure 5.12: Plot of compression-based termination of M4 bolts and Buntline hitch

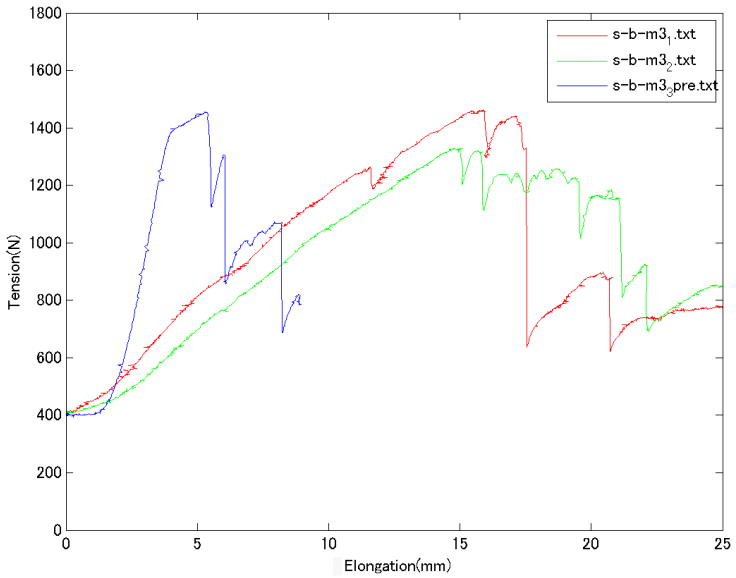

Figure 5.13: Plot of hooking-based termination of M3 bolts and Brummel splice

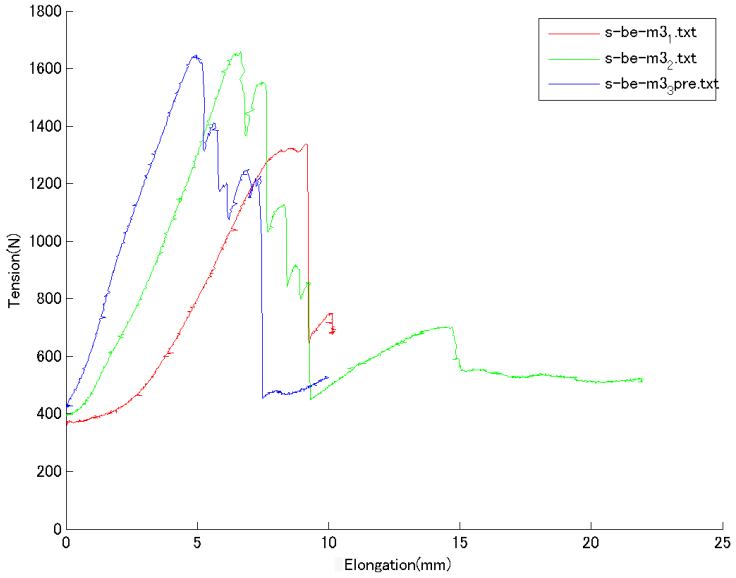

Figure 5.14: Plot of hooking-based termination of M3 bolts and Brummel splice with epoxy

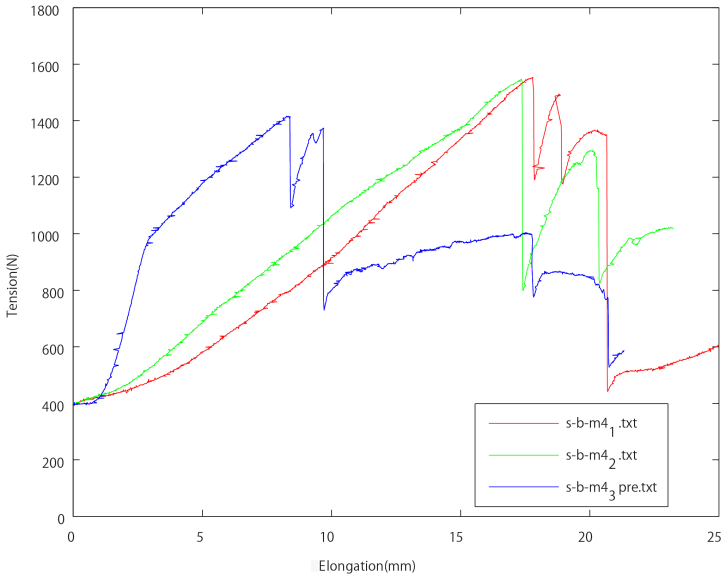

Figure 5.15: Plot of hooking-based termination of M4 bolts and Brummel splice

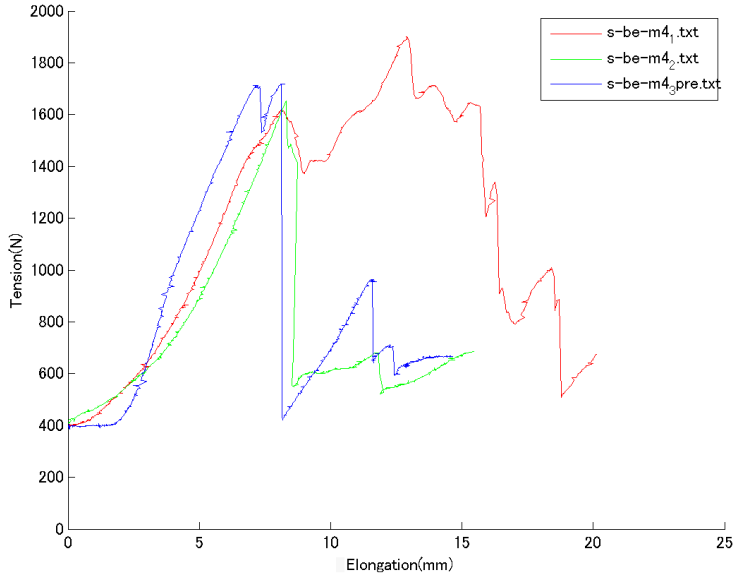

Figure 5.16: Plot of hooking-based termination of M4 bolts and Brummel splice with epoxy

3. Gluing over the knot with epoxy reduced the elongation by almost one-third in any cases.

4. Tendons without compression in the termination structure has higher strength in comparison with the ones with compression. We suspect that the termination with compression prevent the tendons' fibres from rearranging themselves resulting in unbalanced stress among fibres.When any fibres break, the rest support more loads and continuously the whole tendon starts to break.

5. The tendons with M4 termination are slightly stronger than the ones with M3. The cause might come from the different in diameter of the bolts which change the bending angles of tendons. Smaller the diameter is higher the bending angle it becomes. With higher bending angles the distribution of forces among fibres are not uniform resulting in reducing the maximum strength.

Table 5.2: Results from the pulling test in several tendon configurations.

Test code	Average tension (N)	Min. tension (N)	Max. elongation (mm)
f-b-m3	1258	1158	14.6
f-be-m3	1544	1423	8.0
f-b-m4	1493	1347	20.9
f-be-m4	1631	1585	11.5
f-be-m4-d	1154	960	31.5
f-u-m4	1159	1038	29.5
f-bh-m4	1297	1202	25.7
s-b-m3	1412	1328	14.9
s-be-m3	1541	1338	9.1
s-b-m4	1504	1413	17.8
s-be-m4	1751	1651	12.9
s-u-m4	1170	1112	24.9

5.4 Assembly of the Hand Prototype

For the right hand, over 50 parts are printed with 3D-printer and assembled together with machined part, e.g, pulleys, bearings and shafts. During assemblies tendon are routed through the structure as well. The prototype,

not including a wrist and actuators, weights around 350 grams. Figure 5.18 shows the hand viewing from back side and palm side. The curvature on the back surface of the hand covered part of the fingers untill MCP2 joints. The size of hand is similar to the human hand with 195 mm height from the wrist to the tip of middle finger and 110 mm breadth from the thumb to little finger (when thumb is parallel to the other fingers). Palm surface is casted over a 3D-printed part with silicone to increase the grip. Intermediate knots are made to connect tendons from the hand side to the actuator side for the ease of debugging while in the real products we planed to eliminate these connections by knotting Brummel splice on actuators' end as well, the detailed procedures to make Brummel splice with single-ended tendon are described in Section 3.6.2

Figure 5.19 shows the side view of the prototype. Base of the palm is slightly thicker than around MCP2 joints not only for aesthetic purposes, but inside the palm it contains routing mechanism of tendons where outside curvatures are design on top to contain internal structures inside. Figure 5.20 depicts the internal tendon-routing structures inside the palm after the top cover is removed. Tendons from the thumb are painted with colors for the ease of routing process and debugging.

5.5 Linear Actuators

The actuations of our hand are based on linear actuators. Considering of linear actuators, we are aiming at using our Electro-Hydrostatic Actuators (EHAs) which have twelve linear hydraulic cylinders as outputs. EHA [**?**, 28] is a hydrostatic transmission where one-hydraulic motor are driven by one-hydraulic pump that is powered by an electric motor. The main difference when comparing to the conventional hydraulic system is that instead of using servo valves to control the hydraulic motors, hydraulic motors are controlled by pumps directly. Since there is no valves blocking the flow of hydraulic fluid, system becomes backdrivable. Forque/torque measurements can be done easily by using monitoring pressure of hydraulic fluids.

In order to build the test system to compatible with our current developing EHA clusters, we decided to use simple pneumatic system. Actuations are done by twelve cylinders that has 30 mm strokes which are equal to those of EHA clusters. The movements of pneumatic cylinders are controlled by

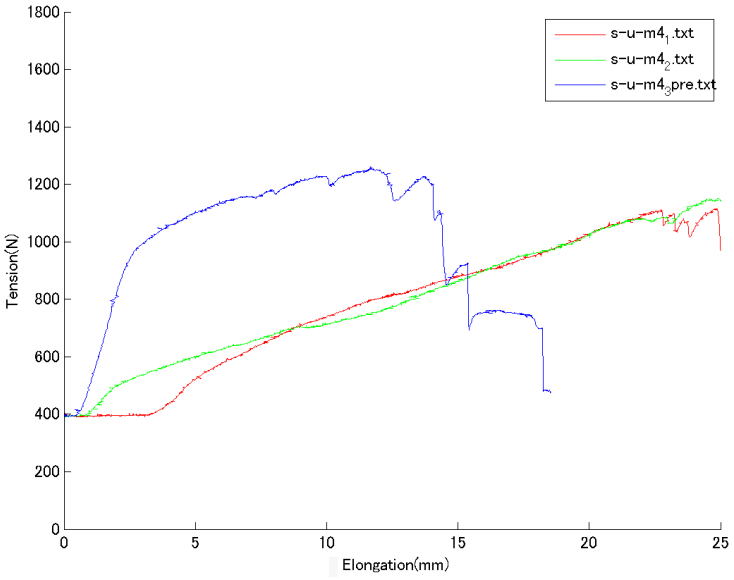

Figure 5.17: Plot of hooking-based termination of M4 bolts and Uniknot

Figure 5.18: The prototype of right hand.

Figure 5.19: Side view of the hand prototype.

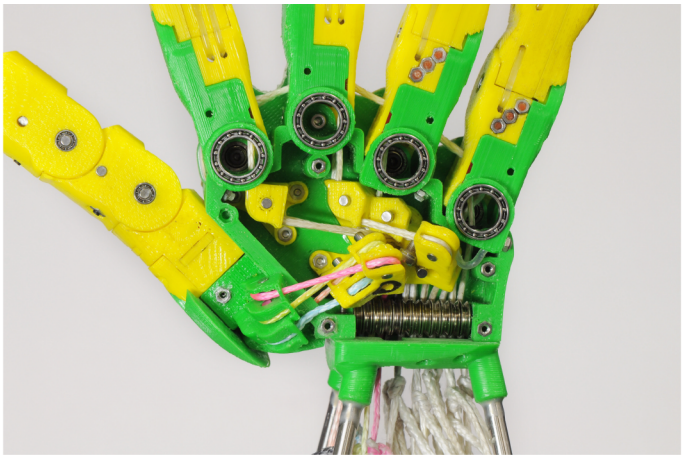

Figure 5.20: Structure inside the palm.

5-way solenoid valves. A control software is programmed on a host computer and communicated with solenoid valves using the EtherCAT™real-time protocol. Since there is no position sensor on the actuators in our setup, we can test only with feed forward control. Figure 5.21 shows the setup of pneumatic system. The right hand prototype with wrist is fixed to twelve pneumatic cylinders and on the right is the cluster of solenoid valves running EtherCAT™protocol. Figure 5.22 depicts the side view of hand prototype. Twelve cylinders are stacked into 3 layers with the maximum of five on each.

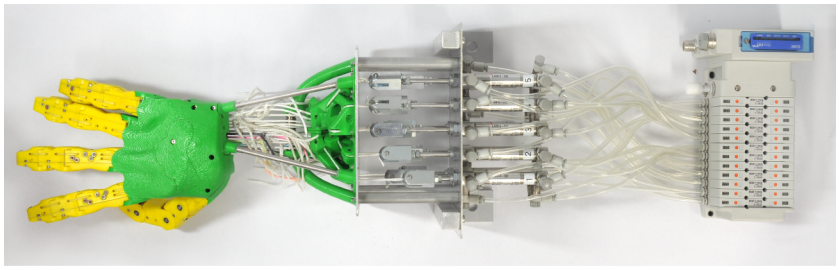

Figure 5.21: Experiment setup with pneumatic actuators and solenoid valves.

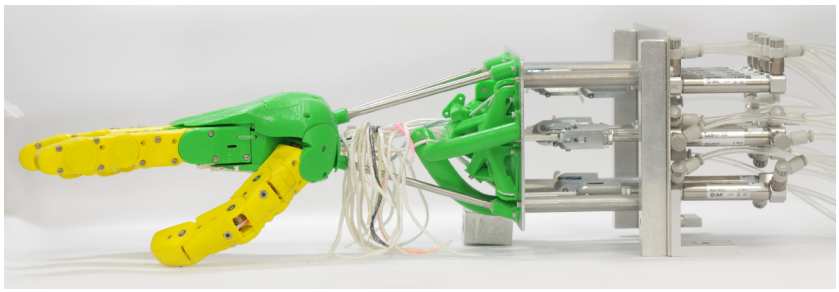

Figure 5.22: Side view of the hand prototype and pneumatic actuators.

5.6 Prototype Hand Experiments

Experiments are divided into 2 sections where the first one we test the movement of our prototype by controlling the motion of each pneumatic actuator. Here, we show video snapshots of each command that is sent to the actuators. Later, we do the motion analysis of an index finger and little finger and discuss about the effects on joint configuration due to our

proposed coupling.

5.6.1 Finger Joint Demonstrations

These demonstrations shows the movement of each degree-of-freedoms (DOF) in the hand. We took video during the experiments and take snapshot images at the end of actuation commands. Snapshots are shown in Figure 5.23 and 5.24. On the right column, names of tendons the are being pulled by actuators are written.

The demonstrations start with initial configuration (Figure 5.23a) where all fingers are fully extended and abducted. Index ,middle, ring, and little finger are at the joint angles determined by minimum potential energy configurations. Since there is no potential function in the thumb, joint configuration must be determined by all five tendons that constraints the joint position. However, there is no feedback position control loop in our pneumatic actuators. Extension of the thumb can be done by sequentially extend TM1, TM2,MCP, and IP joint in order.

MCP2 joint and DIP/PIP joint of index and middle finger can be moved independently (see Figure 5.23b-5.23e) due to the tendons that terminate at MCP2 joint and also the selection of extension spring constant k_{e} and extension spring pretension x_{e}. k_{e} and x_{e} of the MCP2 joints are set to be stronger than that of PIP and DIP joint.

Little and ring finger have one DOF with our proposed coupling for three joints. When actuators pull the tendons, fingers move to the new equilibrium established by minimum potential energy joint configurations. After tendons are pulled to the end (full-stroke), little and ring finger fully flexed, shown in Figure 5.23f-5.23g. Adductions of index, ring and little finger are depicted in Figure 5.23h.

For demonstrations of the thumb, the sequences of actuation to extend the thumb are necessary between each demonstration due to the lack position controllability. Figure 5.24i shows the flexion of IP joint. The range of movement is small before of high static friction in sliding-contact tendon routing between TM1 and TM2 joint. Then, the flexion of MCP joint is shown in Figure 5.24j and later the flexion of TM2 joint is shown in Figure 5.24k. Finally, last DOF of the thumb, adduction of TM1 is demonstrated in Figure 5.24l. Figure 5.24m-5.24o are the combined movement of several joints (Figure 5.24m - TM1/TM2/IP, Figure 5.24n - TM1/MCP, and Figure

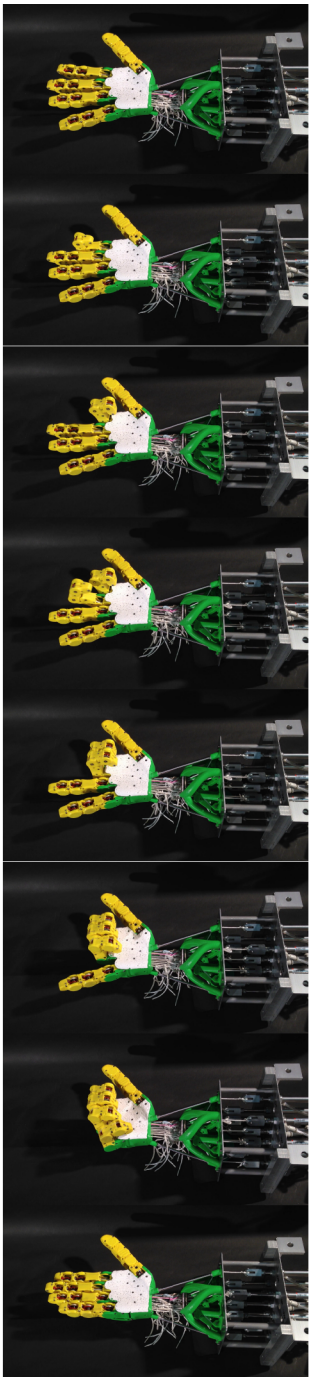

a) Initial configuration

b) Index DIP

c) Index DIP, Index MCP2

d) Index DIP, Index MCP2
Middle DIP

e) Index DIP, Index MCP2
Middle DIP, Middle MCP2

f) Index DIP, Index MCP2
Middle DIP, Middle MCP2
Ring DIP

g) Index DIP, Index MCP2
Middle DIP, Middle MCP2
Ring DIP
Little DIP

h) Adduction

Figure 5.23: Demonstration snapshots of each degree-of-freedom.

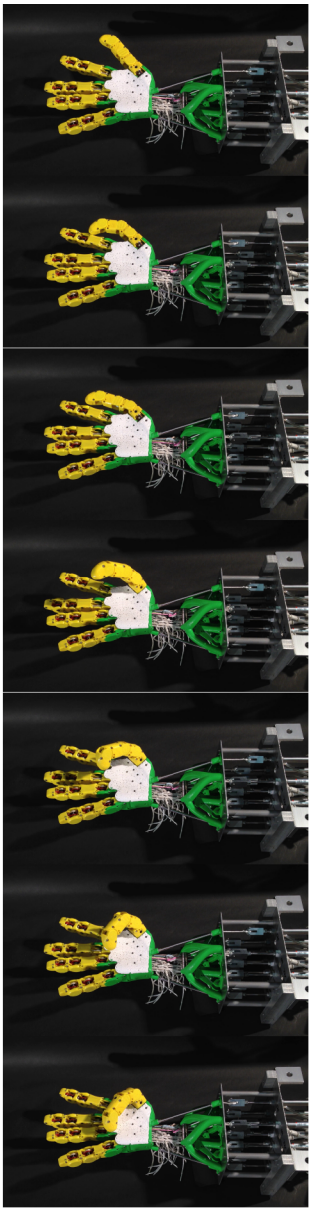

i) Thumb IP2
Thumb MCP

j) Thumb IP1
Thumb IP2

k) Thumb MCP

l) Thumb TM1

m) Thumb IP2
Thumb MCP
Thumb TM1

n) Thumb IP1
Thumb IP2
Thumb TM1
Thumb TM2

o) Thumb IP1
Thumb MCP
Thumb TM1
Thumb TM2

Figure 5.24: Demonstration snapshots of each degree-of-freedom (continue).

5.24o - TM1/TM2).

5.6.2 Motion Analysis of Index Finger and Little Finger

By adding joint angle sensors into the finger, it is possible to study the behaviour of under actuated hands as well as coupling mechanisms. Figure 5.25 shows the assembly of index finger that contains circuit boards for magnetic encoder with SPI daisy-chain communication. SPI daisy-chain connects sensors to SH2A microprocessor development board which is send the data to host PC using Serial communication RS-232, see Figure 5.26. Three joint angles in flexion plane (DIP,PIP,MCP2) are sampled every 100 milliseconds and logged on PC.

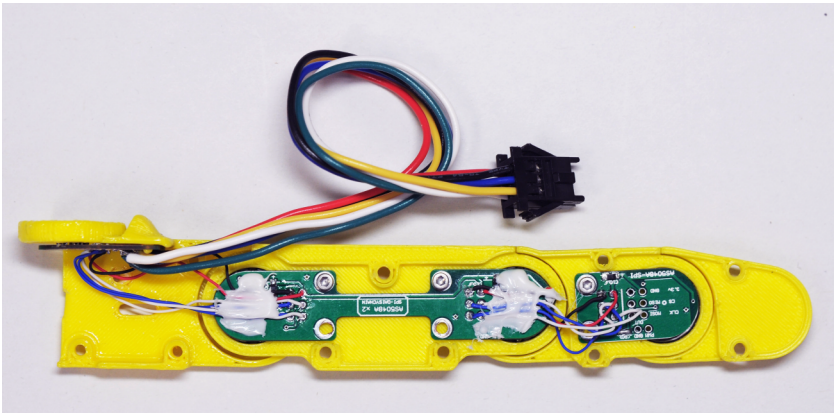

Figure 5.25: Joint angle sensors fitted inside a part of index finger.

Index finger is actuated by only Index DIP tendon while Index MCP2 remains free. The only control over Little finger is the Little DIP tendon. Denoting q_{DIP}, q_{PIP}, and q_{MCP2} as the joint angles at DIP, PIP, and MCP2 joint respectively, we can compute the stroke at actuator (x_{a}) at any joint configurations as follows,

$$x_{\mathrm{a}} = r_{\mathrm{DIP}} q_{\mathrm{DIP}} + r_{\mathrm{PIP}} q_{\mathrm{PIP}} + r_{\mathrm{MCP2}} q_{\mathrm{MCP2}} \tag{5.1}$$

where r_{DIP},r_{PIP}, and r_{MCP2} are the pulley radius at DIP, PIP and MCP2 joint. In these experiment of both index and little finger, all pulleys have the same radius. The joint trajectory versus actuator stroke plots of index finger and little finger are shown in Figure 5.27 and 5.28. Theoretical tra-

jectory of each joints are plot in dotted line. All solid lines plots are data collected from the experiments. Any joint configurations in along the joint trajectory are the minimum point of potential function at given actuation stroke. According to the plot of index finger DIP and PIP joint are 1:1 coupled ($q_{\text{DIP}} = q_{\text{PIP}}$)until they reach the mechanical joint limits around 90 degree then MCP2 joint starts to move. We can observe the hysteresis effect from the actuator that pulled and released the tendon.

DIP, PIP, and MCP2 joint of little finger are coupled. In theory, the joint trajectory at any given actuation stroke would result in $q_{\text{DIP}} = q_{\text{PIP}} = q_{\text{MCP2}}$ while the same tendency can be observe from this experiment. Therefore, we can recognize this tendency from the joint trajectory plot of little finger. Hysteresis behaviour on little finger seems to be more than that on index finger because 3-joint coupling, implemented on little finger, requires more complex tendon routing resulting in larger static coulomb friction.

We can also plot the forward kinematic chains of index and little finger by using the joint trajectories. The forward kinematic plots of index and little are shown in Figure 5.29 and 5.30. Experiments start with configurations shown in orange and after tendons are full at full stroke fingers end up at the configuration drawn in red. It can be observed that for index finger PIP and DIP are coupled at the beginning while MCP2 joint remain zero but after PIP and DIP reach the joint limit MCP2 starts to rotate while on little finger DIP, PIP, and MCP2 are trying to track the minimum potential trajectory $q_{\text{DIP}} = q_{\text{PIP}} = q_{\text{MCP2}}$.

The second experiments are done to prove an underactuated capability of the design. Figure 5.31 and 5.32 are the trajectory plots when the actuator position is fixed to 7.3 mm for index finger and 10.6 mm for little finger. An underactuation happens when there are external forces acting on the finger resulting in the new equilibrium configuration which is still the minimum potential configuration. The new equilibrium configuration depends on direction and location of external forces. Theoretical trajectory for all underactuated joints must lie on the line x = 7.3 and 10.6 accordingly. Deviations of the trajectory results from the experiment are expected to come from slackness of an actuation tendon. Once the external forces are released fingers move back to the unique equilibrium configuration given actuator stroke, shown in black and white dots.

Using the joint trajectories from second experiment, we can plot forward

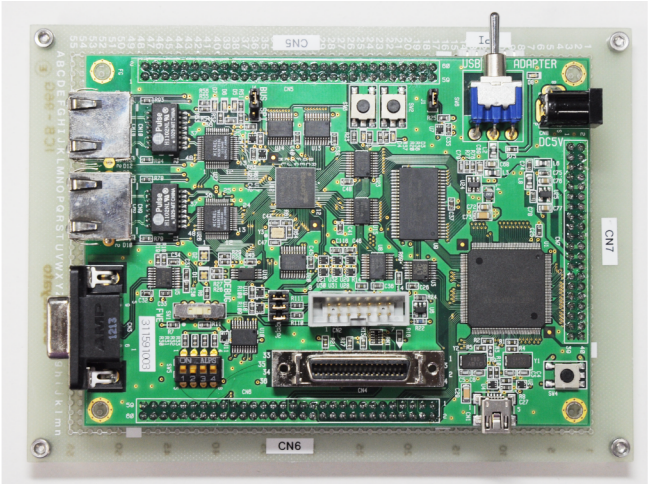

Figure 5.26: Renesas SH2A microprocessor development board.

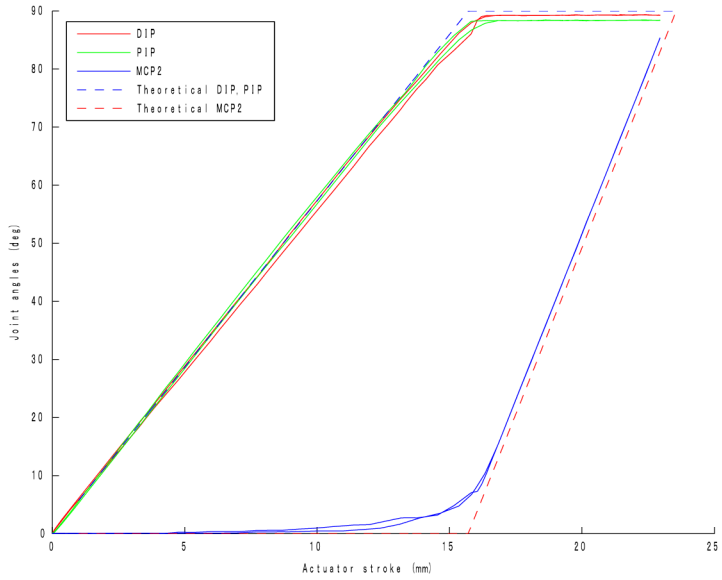

Figure 5.27: Equilibrium joint trajectory of index finger.

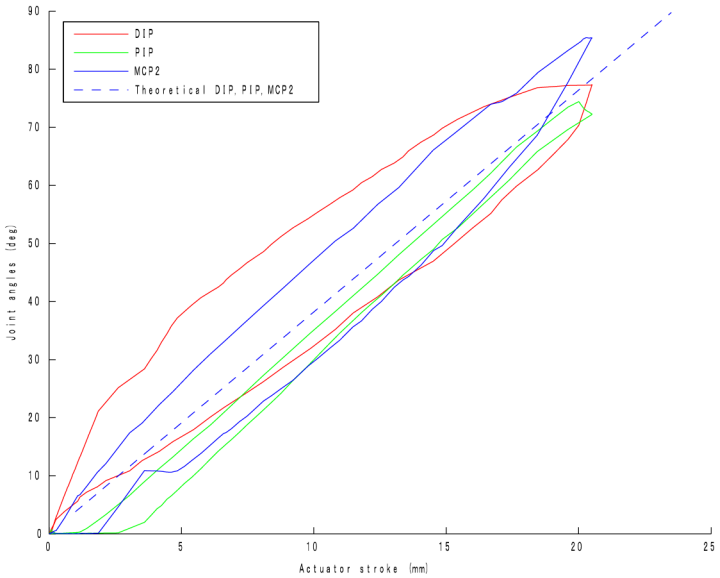

Figure 5.28: Equilibrium joint trajectory of little finger.

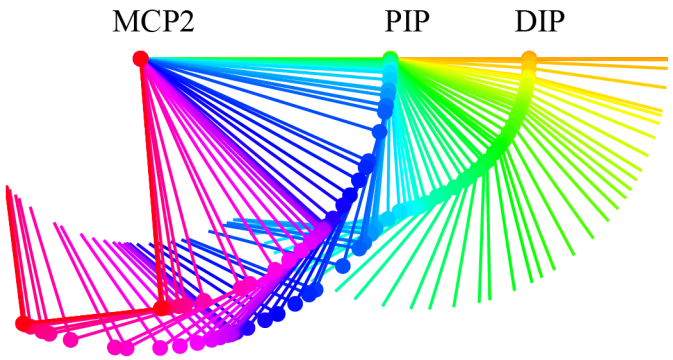

Figure 5.29: Forward kinematics of index finger's equilibrium configuration.

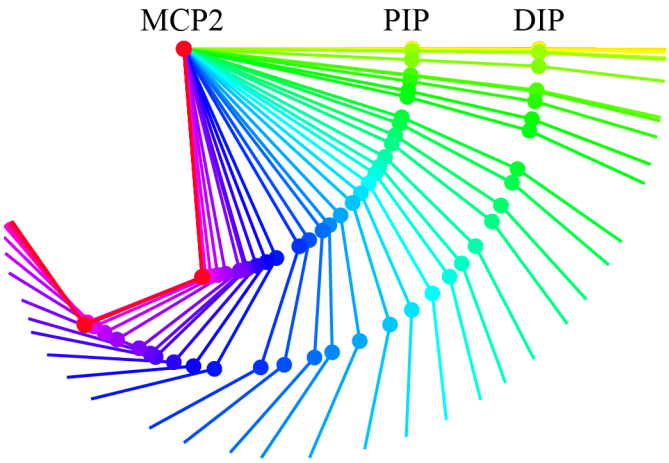

Figure 5.30: Forward kinematics of little finger's equilibrium configuration.

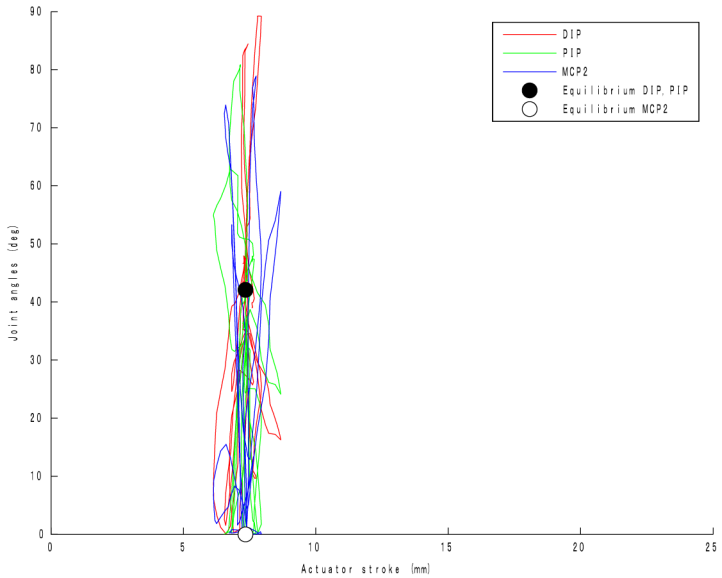

Figure 5.31: Underactuated behaviour of index finger at fixed tendon length (7.3 mm).

kinematic chain of index finger and little finger as shown in Figure 5.33 and 5.34.

In the second experiment for both index and little finger, 3 joints are constrained by the only one active tendon resulting in two underactuated DOFs. These extra DOFs allow changes in joint configurations depend on the external force. The constrain given by one fixed length active tendon can be written as below,

$$c = r_{\mathrm{DIP}} q_{\mathrm{DIP}} + r_{\mathrm{PIP}} q_{\mathrm{PIP}} + r_{\mathrm{MCP2}} q_{\mathrm{MCP2}} \tag{5.2}$$

where c is the constant length actuation tendon which is 7.3 mm and 10.6 for the experiment on index and little finger. It is possible to plot a plane in 3-joint space that is given by the constrain in equation 5.2. The resulting plots are shown in Figure 5.35 and 5.36. White dots are the joint configurations that has minimum potential energy at a given experiment setup. Blue dots are joint configurations when external forces exerted on the system. Red planes are the theoretical plane of all possible joint configurations for underactuated finger. We can observe that most of the blue dots lie along the red plane which explain the constraint given by fixed actuator stroke while some outliers can be explained by slackness of the actuation tendons.

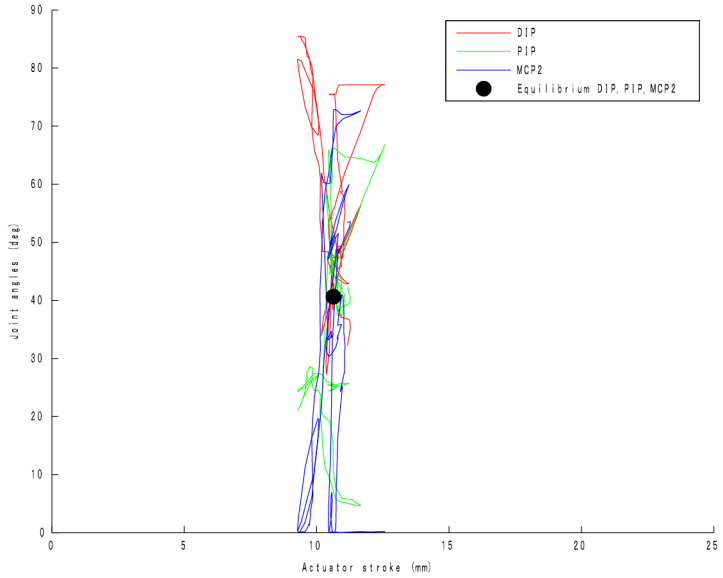

Figure 5.32: Underactuated behaviour of little finger at fixed tendon length (10.6 mm).

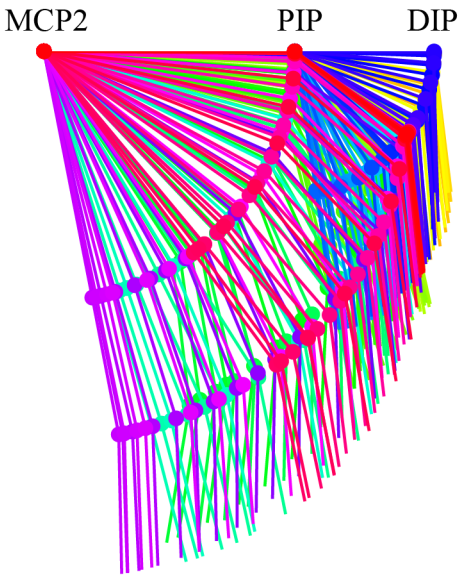

Figure 5.33: Forward kinematics of underactuated index finger at fixed tendon length (7.3 mm).

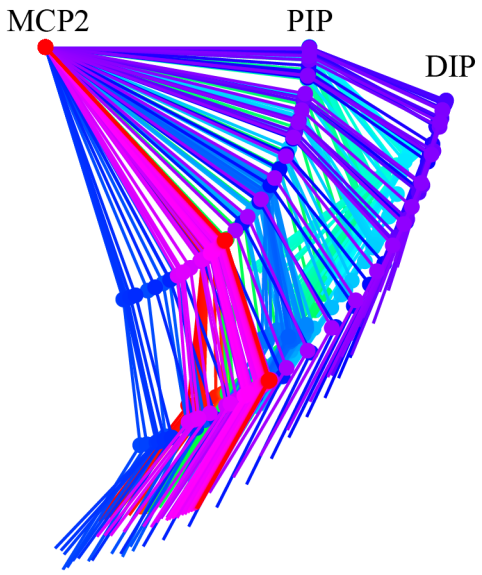

Figure 5.34: Forward kinematics of underactuated little finger at fixed tendon length (10.6 mm).

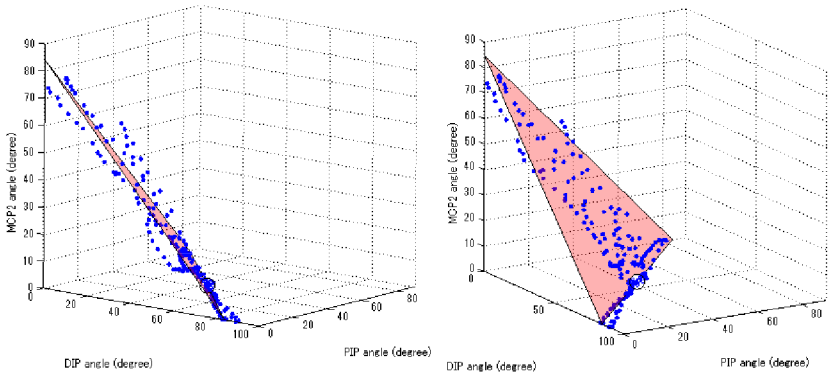

Figure 5.35: Joint angle plot of underactuated index finger at fixed tendon length (7.3 mm).

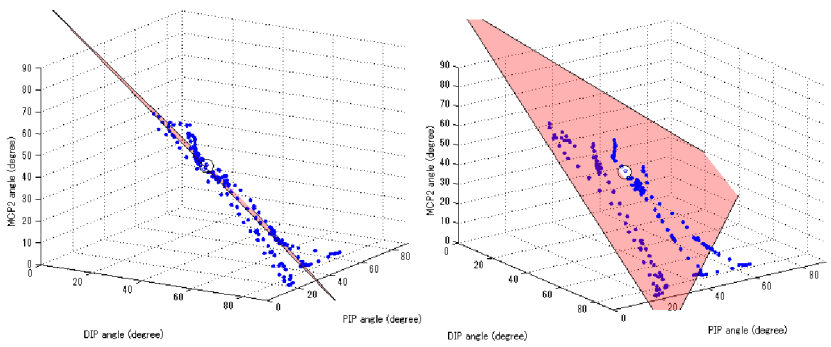

Figure 5.36: Joint angle plot of underactuated little finger at fixed tendon length (10.6 mm).

Chapter 6

Conclusion

In this thesis we proposed the design of anthropomorphic robot hand . The proposed design has 12 degree-of-freedom. By the end a prototype has been made using rapid prototyping technology that breaks the limitation of complicated shapes which are difficult to build with any conventional machining techniques.

At beginning we reviewed the mathematical model for tendon-driven mechanism which is very useful for later discussions. Some of the previous design of robot hand are classify into categories. We also discussed about the coupling mechanism for underactuated hands by analysing the joint equilibrium configurations. We looked at the physiology of human hand as an inspiration of our anthropomorphic design which not only having similar sizes and shapes as human hand but also capable of performing the similar grasping functionalities as well. To do so, we carefully selected the placement of active DOFs in our simplified model of human hand, resulting in twelve-DOF robot hand. To achieve the joint space controllability of underactuated hand, we proposed a new coupling design that enables the separation of passive tendons for coupling and for extension purposes. We developed 3-dimensional pulley system that is aimed for reducing the frictions. As a result, we designed a free-form shape in 3D space that cannot be build by any material-removal machining process. This emphasize the usefulness of rapid prototyping technology. We discussed the detailed design of each fingers, palm and wrist, as well as, joint angle sensors. Choices of tendon and termination mechanism are tested to find the proper way to fix the tendon. The prototype of five-finger 12-DOF underactuated hand has been built and

the demonstrations of each degree-of-freedom motion are shown. We also analysed the behaviour of the proposed underactuated hand by using joint angle sensors that are integrated inside the fingers.

As future works, it would be interesting to do grasping experiments over variety of objects especially pinching with fingertips to prove the use of our proposed coupling compared to the common design of underactuated hand. Since the pneumatic system that we are using right now is not capable of feedback position control, we are planning to install all joint encoder to roughly estimate the position of each actuator and perform more precise control. Currently we are developing a cluster of 14 Electro-Hydrostatic Actuators(EHAs) for the actuation of the hand and wrist. In near future, we will replace pneumatic cylinders with EHAs which are capable of performing high output forces and precise position/force control. Twelve actuators will be use for twelve-DOF hand and the other two for two-DOF wrist. The design of wrist has to take in to account as well which is still the future work at this current stage. More in the theoretical senses, more intensive analysis on the behaviour of underactuated hand must be done. The grasping simulators for underactuated hand are essential to study the planning of underactuated hand.

In terms of manufacturing techniques, we are searching for other rapid prototyping technologies, for example, Selective Laser Sintering and Stereolithography, that enable the use of other materials like metal or acrylic. More importantly, by combining rapid prototyping technologies with other conventional process such as, machining, casting, or injection, it is possible to explore the new spaces of mechanical design which are impossible by using single technique.

Acknowledgements

I would like to express my special thank to Professor Yoshihiko Nakamura who give me one of the greatest opportunity in my life to study here in The University of Tokyo. Japan, at least for me, is one of the dream place I want to visit, nice city and long-lasting culture. That is my imagination before coming here. I did not even know what is the meaningful of research. For almost 2 years and a half that I spend in this lab I found that the tough I had before is just a small part of Japan that is visible to foreigner like me. Staying in this lab really teaches me the essence of Japanese where people devoted their life to achieve the excellent work results from the ambitious inside. During this two year Nakamura-sensei gave me lots of question about my research that indeed pushing me towards how to think logically and how he looks at my work as a very-well experienced professional researcher.

This thesis cannot complete if I did not know Professor Hiroshi Kaminaga. From his out-look he is a very direct person but once I get to work with him I feel that he is one of the very generous Japanese guy. I am always interested by the mechanics since I was a child. I need to thank to my father who is paediatrician who always do some DIY projects at home. I learned a lot from his DIY experiences even though my education background has not thing to do with Mechanical Engineer. At first I was so nervous to bet my master thesis on something I had never studied before but Kaminaga-sensei kindly introduce me to the whole new world of Mechanics. Kaminaga-sensei is indeed the most practical guy I knew since I was born. He teaches me not only how to build things but also how to build it like professional. I was so surprised that anytime I show him my works he always give me a very useful comment right to the spot. I truly appreciate Kaminaga-sensei.

Professor Wataru Takano who always stay very late in the lab. He always encourage me when I feel exhausted from the research. Professor

Hok Ayusawa as well as Professor Akihiko Murai, they both are very kind and they are the real hard workers. Without them, I would be so lonely when I need to come work on the weekend. Mika Ueno, our lab's secretary who take care of my paper works and more importantly she taught me to be humble.

Professor Antonio Bicchi (University of Pisa, Italy), Professor Donheui Lee (TUM, German), and Doctor Christian Ott (DLR, German), they kindly give me an opportunity to visit the world's leading research lab in Robotics which give me the invaluable in-touch experiences that give lots of inspiration afterwards. My 25 days Europe trip is kindly supported by our Graduate school of IST, The University of Tokyo.

I had great experiences with all members of YNL. Since my very first day in Japan, my tutor Kanade Kubota took care of all my paper works. Risto Kaijaluoto, a research student from Finland, who entered this lab almost at the same time as me. We had very nice experiences together by sharing the same deadlines. One of the member who is working closely with me which I cannot skip mentioning is Tianyi Kang or Ko-kun. He is working on the design of EHA actuator for my robot hand in which we need to share lots of information. He gives me plenty of advices on my work as a real mechanical engineer. One of my best friend in YNL is of course Caron Stephane. We share not only working moments in the lab but also life and interests. As far as I know, he is among the fastest linux users and as well as a very good programmer. Carlos Felipe Santacruz is a good example for not only hard-working but also how to keep you body firm. He also inspired me to start jogging in the evening to keep myself healthy. Quang-Coung Pham is the postdoc researcher at the time I arrived. Coung gave me a very warm chat just like my long-known senior. Even though we work on the totally different topics, I always very impressed by his works. Sometimes I played badminton with Matthew Howard and thanks to Manish Sreenivasa who bring us to the Volunteer activity in Ishinomaki after the Nuclear disaster in 2011. I really appreciate his devotion on helping other people. I like talking with Nierhoff Thomas who shares the same interest on bicycles.

During the time in the lab, I enjoy Japanese conversation with my second Japanese teachers, Seiya Hamano, Hirokaza Tanaka, Kouhei Odanaka, Kohei Hiromatsu, Akihiro Yoshimatsu, Keisuke Umesawa, Satoshi Otsuki, Kensyou Hirasawa, Yuuta Andoh, Kazanari Takeichi, Ryo Masumura, and

Yuusuke Gohtsu. International students, ChangHeon Yi, Sabastien Cagnon, Shun-Chieh Hung, and Paul Mathieu who helps me adapting my self to the lab environment and advice me how to study for the entrance examination.

My study in Japan would not be possible without the support from the Japanese government (MEXT). I want to thank to many Japanese teachers from both the Japanese Language Center of TODAI as well as language courses providing by School of Engineering. Without those Japanese knowledges, life here would not be these fruitful and rewarding.

My life and study are coupled in some senses, many times when I had problems, I always think of my mom who knows me best in the world. She does not hesitate to pick up my call even in the middle of the night. I cannot believe that just few words from her can solve the whole problem. I would like to thank to lots of my friends to make living here very colorful. My best friends, Gig, Vee, Boss, Tum, Ann, and Joy, we always spend most of the weekend together. They are always there to help when I feel discourage. P'Ja, P'Ping, P'Veen, and P'Klui are my seniors who arrange lots of activities to keep us connected and becomes friends. Pinn, Ole, Golf, N'Kaew, N'Pop, N'Mint are friends who we share lots of experiences.

Bibliography

[1] George A Bekey, Rajko Tomovic, and Ilija Zeljkovic. Control architecture for the belgrade/usc hand. In *Dextrous robot hands*, pages 136–149. Springer, 1990.

[2] Christopher Y Brown and H Harry Asada. Inter-finger coordination and postural synergies in robot hands via mechanical implementation of principal components analysis. In *Intelligent Robots and Systems, 2007. IROS 2007. IEEE/RSJ International Conference on*, pages 2877–2882. IEEE, 2007.

[3] Marco Gabiccini, Antonio Bicchi, Domenico Prattichizzo, and Monica Malvezzi. On the role of hand synergies in the optimal choice of grasping forces. *Autonomous Robots*, 31(2-3):235–252, 2011.

[4] Haruhisa Kawasaki, Tsuneo Komatsu, and Kazunao Uchiyama. Dexterous anthropomorphic robot hand with distributed tactile sensor: Gifu hand ii. *Mechatronics, IEEE/ASME Transactions on*, 7(3):296–303, 2002.

[5] Kenji Kaneko, Kensuke Harada, Fumio Kanehiro, Gou Miyamori, and Kazuhiko Akachi. Humanoid robot hrp-3. In *Intelligent Robots and Systems, 2008. IROS 2008. IEEE/RSJ International Conference on*, pages 2471–2478. IEEE, 2008.

[6] Jörg Butterfaß, Markus Grebenstein, Hong Liu, and Gerd Hirzinger. Dlr-hand ii: Next generation of a dextrous robot hand. In *Robotics and Automation, 2001. Proceedings 2001 ICRA. IEEE International Conference on*, volume 1, pages 109–114. IEEE, 2001.

[7] S.C. Jacobsen, E.K. Iversen, D. Knutti, R. Johnson, and K. Biggers. Design of the utah/m.i.t. dextrous hand. In *Robotics and Automation.*

Proceedings. 1986 IEEE International Conference on, volume 3, pages 1520–1532, 1986.

[8] Markus Grebenstein, Alin Albu-Schaffer, Thomas Bahls, Maxime Chalon, Oliver Eiberger, Werner Friedl, Robin Gruber, Sami Haddadin, Ulrich Hagn, Robert Haslinger, et al. The dlr hand arm system. In *Robotics and Automation (ICRA), 2011 IEEE International Conference on*, pages 3175–3182. IEEE, 2011.

[9] Giorgio Grioli, Manuel Catalano, Emanuele Silvestro, Simone Tono, and Antonio Bicchi. Adaptive synergies: an approach to the design of under-actuated robotic hands. In *Intelligent Robots and Systems (IROS), 2012 IEEE/RSJ International Conference on*, pages 1251–1256. IEEE, 2012.

[10] George A Bekey, Rajko Tomovic, and Ilija Zeljkovic. Control architecture for the belgrade/usc hand. In *Dextrous robot hands*, pages 136–149. Springer, 1990.

[11] M Catalano, G Giorgio, A Serio, E Farnioli, C Piazza, and A Bicchi. Adaptive synergies for a humanoid robot hand. In *IEEE–RAS international conference on humanoid robots*, 2012.

[12] Long Wang, Joseph DelPreto, Sam Bhattacharyya, Jonathan Weisz, and Peter K Allen. A highly-underactuated robotic hand with force and joint angle sensors. In *Intelligent Robots and Systems (IROS), 2011 IEEE/RSJ International Conference on*, pages 1380–1385. IEEE, 2011.

[13] Aaron M Dollar and Robert D Howe. Joint coupling design of underactuated hands for unstructured environments. *The International Journal of Robotics Research*, 30(9):1157–1169, 2011.

[14] I.A. Kapandji. *The physiology of the joints*. Number v. 3 in The Physiology of the Joints. Churchill Livingstone, 2008.

[15] Anne Hollister, William L Buford, Loyd M Myers, David J Giurintano, and Andrew Novick. The axes of rotation of the thumb carpometacarpal joint. *Journal of Orthopaedic Research*, 10(3):454–460, 1992.

[16] J Salisbury. Design and control of an articulated hands. In *Proc. of the International Symposium on Design and Synthesis*, 1984.

[17] CS Lovchik and Myron A Diftler. The robonaut hand: A dexterous robot hand for space. In *Robotics and Automation, 1999. Proceedings. 1999 IEEE International Conference on*, volume 2, pages 907–912. IEEE, 1999.

[18] Myron A Diftler, JS Mehling, Muhammad E Abdallah, Nicolaus A Radford, Lyndon B Bridgwater, Adam M Sanders, Roger Scott Askew, D Marty Linn, John D Yamokoski, FA Permenter, et al. Robonaut 2-the first humanoid robot in space. In *Robotics and Automation (ICRA), 2011 IEEE International Conference on*, pages 2178–2183. IEEE, 2011.

[19] Shadow Robot Company. The shadow dexterous hand. http://www.shadowrobot.com/products/dexterous-hand/, 2013.

[20] Markus Grebenstein, Maxime Chalon, Gerd Hirzinger, and Roland Siegwart. Antagonistically driven finger design for the anthropomorphic dlr hand arm system. In *Humanoid Robots (Humanoids), 2010 10th IEEE-RAS International Conference on*, pages 609–616. IEEE, 2010.

[21] Ryuta Ozawa, Kazunori Hashirii, and Hiroaki Kobayashi. Design and control of underactuated tendon-driven mechanisms. In *Robotics and Automation, 2009. ICRA'09. IEEE International Conference on*, pages 1522–1527. IEEE, 2009.

[22] DSM Company. Dyneema. http://www.dyneema.com/, 2013.

[23] Hayami Industry Company. Super cord. http://www.hayami.co.jp /hamilon_english/products/super_cord.html, 2013.

[24] Stratasys company. Dimension sst 1200. http://www.stratasys.com/3d-printers/design-series/performance/dimension-1200es, 2013.

[25] Grog LLC Company. Brummel splice. http://www.animated knots.com/brummel/, 2013.

[26] Grog LLC Company. Duncan (uni) knot. http://www.animated knots.com/uniknot/, 2013.

[27] Grog LLC Company. Buntline hitch. http://www.animated knots .com/buntline/, 2013.

[28] Hiroshi Kaminaga, Junya Ono, Yuto Shimoyama, Tomoya Amari, Yukihiro Katayama, and Yoshihiko Nakamura. Anthropomorphic robot hand with hydrostatic cluster actuator and detachable passive wire mechanism. In *Humanoid Robots, 2009. Humanoids 2009. 9th IEEE-RAS International Conference on*, pages 1–6. IEEE, 2009.

以上

修 士 論 文

平成 25年 8月 16日 提出

116557　　トリーラッタナクンワオン　タナット
Treratanakulwong, Tanut